

# Inference of Co-Evolving Site Pairs: an Excellent Predictor of Contact Residue Pairs in Protein 3D structures

Sanzo Miyazawa

Graduate School of Engineering, Gunma University, Kiryu, Gunma 376-8515, Japan

E-mail: sanzo.miyazawa@gmail.com

## Abstract

Residue-residue interactions that fold a protein into a unique three-dimensional structure and make it play a specific function impose structural and functional constraints on each residue site. Selective constraints on residue sites are recorded in amino acid orders in homologous sequences and also in the evolutionary trace of amino acid substitutions. A challenge is to extract direct dependences between residue sites by removing indirect dependences through other residues within a protein or even through other molecules. Recent attempts of disentangling direct from indirect dependences of amino acid types between residue positions in multiple sequence alignments have revealed that the strength of inferred residue pair couplings is an excellent predictor of residue-residue proximity in folded structures. Here, we report an alternative attempt of inferring co-evolving site pairs from concurrent and compensatory substitutions between sites in each branch of a phylogenetic tree. First, branch lengths of a phylogenetic tree inferred by the neighbor-joining method are optimized as well as other parameters by maximizing a likelihood of the tree in a mechanistic codon substitution model. Mean changes of quantities, which are characteristic of concurrent and compensatory substitutions, accompanied by substitutions at each site in each branch of the tree are estimated with the likelihood of each substitution. Partial correlation coefficients of the characteristic changes along branches between sites, in which linear dependences on other sites are removed, are calculated and used to rank co-evolving site pairs. Accuracy of contact prediction based on the present co-evolution score is comparable to that achieved by a maximum entropy model of protein sequences for 15 protein families taken from the Pfam release 26.0. Besides, this excellent accuracy indicates that compensatory substitutions are significant in protein evolution.

## Introduction

The evolutionary history of protein sequences is a valuable source of information in many fields of science not only in evolutionary biology but even to understand protein structures. Residue-residue interactions that fold a protein into a unique three-dimensional (3D) structure and make it play a specific function impose structural and functional constraints on each amino acid. Selective constraints on amino acids are recorded in amino acid orders in homologous protein sequences and also in the evolutionary trace of amino acid substitutions. Negative effects caused by mutations at one site must be compensated by successive mutations at other sites [1–4], otherwise negative mutants will be eliminated from a gene pool and never reach fixation in a population. Such structural and functional constraints arise from interactions between sites mostly in close spatial proximity. Thus, it is suggested that the types of amino acids and amino acid substitutions must be correlated between sites that are close in a protein 3D structure [5–18]. However, correlations of amino acid types and amino acid substitutions do not only reflect direct interactions between sites but also indirect ones through other residues within a protein or even through other molecules involved in a molecular complex [19, 20] such as oligomerization [16], protein-substrate, protein-protein [18], and protein-DNA. In addition, statistical noise due to the small number of samples and methodological limitations are obstacles to decode correlations into spatial relationships between sites. However, protein families consisting of homologous sequences in a wide range of divergence are now collected in protein family databases such as Pfam [21], and become available to reduce statistical noise to

a sufficiently small amount. A present challenge is thus to extract only direct dependences between sites by excluding indirect correlations between them from a wide variety of homologous sequences evolutionarily exploited in a sequence space [22–27].

Extracting essential information from the evolutionary sequence record have been attempted using global statistical models. A Bayesian graphical model was applied to disentangling direct from indirect dependencies between residue positions in multiple sequence alignments of proteins [23], and a significant improvement was achieved in the accuracy of contact prediction [24]. A Bayesian graphical model was also applied to the analysis of the joint distribution of substitution events to identify significant associations among residue sites [22]. Recently, remarkable accuracy of contact prediction was achieved [25, 26] by using a maximum entropy model [18] of a protein sequence, constrained by the statistics of a multiple sequence alignment, to infer residue pair coupling. Partial correlation coefficients derived from mutual information of residue pair coupling were also used to extract direct information [27]. They developed not only a robust method to extract essential correlations of amino acid type between residue positions in multiple sequence alignments, but also showed that inferred residue-residue proximities provide sufficient information to predict a protein fold without the use of known three-dimensional structures.

Here, we report an alternative approach of inferring co-evolving site pairs from concurrent and compensatory substitutions between sites in each branch of a phylogenetic tree. First, branch lengths of a phylogenetic tree inferred by the neighbor-joining (NJ) method [28] are optimized by maximizing a likelihood of the tree in a mechanistic codon substitution model [29, 30]. The variation of selective constraints over sites is approximated by a discrete gamma distribution [31]. Mean changes of the various types of quantities, which are characteristic of concurrent and compensatory substitutions, accompanied by substitutions at each site in each branch of the tree are estimated on the basis of likelihoods. Partial correlation coefficients of their characteristic changes accompanied by substitutions along branches between sites are employed to remove a linear dependence on characteristic changes along branches at other sites. In other words, a Gaussian graphical model [32] is assumed for site dependence, because a conditional independence between two variables given other variables in a multi-variate Gaussian distribution is equivalent to zero partial correlation coefficient between the two variables. Then, co-evolution scores are defined from partial correlation coefficients of the various types of the characteristic quantities. Co-evolving site pairs are inferred in the decreasing order of the overall co-evolution score. Accuracy of contact prediction based on the partial correlation coefficients is comparable to that by a maximum entropy model [26] for 15 protein families taken from the Pfam release 26.0 [21], indicating that the present method can be an alternative approach for contact prediction. Also, a fact that contact site pairs can be well predicted by the present method strongly indicates that compensatory substitutions are significant in protein evolution, because the present method based on concurrent and compensatory substitutions will not work at all if all substitutions are completely neutral.

## Results

### Framework of the present method

The framework of the present method is shown in Fig. 1. For each protein family, its phylogenetic tree  $T$  inferred by the neighbor-joining (NJ) method is taken from the Pfam database [21] and branch lengths  $t_b$  of the tree are optimized by maximizing the likelihood of the tree in a mechanistic codon substitution model. Then, the average changes ( $\Delta_{ib}$ ) of quantities, which are characteristic of concurrent and compensatory substitutions, accompanied by substitutions at each site  $i$  in each branch  $b$  of the phylogenetic tree  $\hat{T}$  are estimated with the likelihood of each substitution. Their correlation coefficients ( $r_{\Delta_i \Delta_j}$ ) along branches between sites are calculated, and converted to partial correlation coefficients,

which are correlation coefficients between residual vectors ( $\Pi_{\perp\{\Delta_{k \neq i,j}\}}\Delta_i$  and  $\Pi_{\perp\{\Delta_{k \neq i,j}\}}\Delta_j$ ) of given two vectors that are perpendicular to a subspace consisting of other vectors except those two vectors ( $\Delta_i$  and  $\Delta_j$ ) and therefore cannot be accounted for by a linear regression on other vectors. Finally, co-evolution scores based on the partial correlation coefficients are defined and used to rank site pairs for close spatial proximity.

The following characteristic changes defined in the Methods section are examined to detect concurrent and compensatory substitutions between sites; (1) occurrence of amino acid substitution:  $\Delta_i^s$ , (2) side-chain volume:  $\Delta_i^v$ , (3) side-chain charge:  $\Delta_i^c$ , (4) hydrogen-bonding capability:  $\Delta_i^{hb}$ , (5) hydrophobicity:  $\Delta_i^h$ , (6)  $\alpha$  propensity:  $\Delta_i^\alpha$ , (7)  $\beta$  propensity:  $\Delta_i^\beta$ , (8) turn propensity:  $\Delta_i^t$ , (9) aromatic interaction:  $\Delta_i^{ar}$ , (10) branched side-chain:  $\Delta_i^{br}$ , (11) cross-link capability:  $\Delta_i^{cl}$ , and (12) ionic side-chain:  $\Delta_i^{ion}$ . All except the  $\alpha$  propensity are used to define co-evolution scores.

## Protein families and sequences used

In order to calculate partial correlation coefficients between sites by taking the inverse of a covariance or correlation matrix, it must be regular so that the number of homologous sequences must be at least more than the number of sites, that is, the sequence length. To obtain statistically reliable numbers, even more sequences than 10 times as many as sites would be needed. In the Pfam database [21], protein domain families consisting of many thousands of homologous sequences are included. Particularly, protein domain families used in [26] to infer residue pair couplings in multiple sequence alignments are appropriate to allow us to compare prediction accuracies between the present method and their method. These protein domain families in the Pfam release 26.0 (November 2011) are listed in Table 1. Also, Table 1 shows the Uniprot ID and corresponding protein coordinates (PDB ID) of a target protein in each protein family, for which co-evolving site pairs are predicted.

In the Pfam database, there are two sets of sequence alignments for each protein family; a seed alignment and a full alignment. Also, a phylogenetic tree inferred from each alignment by the NJ method [28] are available. Here the seed alignment and its phylogenetic tree are used to estimate parameters in a mechanistic codon substitution model [29, 30]. With those parameters optimized for the seed alignment in the codon-based model, posterior means of characteristic variables at each site in each branch of a phylogenetic tree are estimated for subsets of a full alignment, after branch lengths are optimized.

The full alignments include closely-related sequences whose differences are less than 0.01. The number of branches ( $n_b$ ) in a phylogenetic tree is proportional to the number of OTUs ( $n_{otu}$ ) (operational taxonomic units that correspond to sequences in the present case);  $n_b = 2n_{otu} - 3$  for an unrooted tree. Computational time required for the present calculation increases with increasing number of branches. Including closely-related sequences requires computationally intensive calculation, although it is not much informative; invariant sites do not have any information in the present method, which is designed to detect concurrent and compensatory substitutions between sites in proteins. Thus, subsets made by excluding closely-related sequences from the Pfam full alignments are used in the present calculations. The subsets of a full alignment and their NJ trees are made by removing OTUs that are connected to the parent nodes with branches shorter than a certain threshold ( $T_{bt}$ ), although seed sequences and a target protein are not removed.

In addition, to reduce a computational load in the calculation of the likelihood of a phylogenetic tree, only site positions where amino acids are found in the target protein are extracted from the multiple sequence alignment and used in the present analysis.

## Correlation versus partial correlation coefficients

First, we examined how differently correlation coefficients and partial correlation coefficients between sites identify dependent site pairs. The distribution of Pearson's correlation coefficient in the case of no correlation can be well approximated by the Student's  $t$  distribution. Therefore, here a correlation coefficient  $r_t$  corresponding to the E-value  $E_t = 0.001$  (the P-value  $P_t = E_t/n_{\text{pairs}}$ ) in the Student's  $t$ -distribution of the degree of freedom  $df = n_b - 2$  is used as a threshold for significance; where  $n_{\text{pairs}}$  is the number of site pairs and  $n_b = 2n_{\text{otu}} - 3$  is the number of branches in a unrooted phylogenetic tree.

In Table 2, correlation coefficients ( $r_{\Delta_i^s \Delta_j^s}$ ) and partial correlation coefficients ( $r_{\Pi_{\perp} \Delta_i^s \Pi_{\perp} \Delta_j^s}$ ) of substitution probabilities along branches between sites are classified into four categories; significantly positive, positive but insignificant, negative but insignificant, significantly negative. In addition, sites pairs in each category are classified according to whether they are contact residue pairs in the protein 3D structure. Contact residue sites are arbitrarily defined as residue pairs whose minimum atomic distances are shorter than 5Å, and which are separated by 6 or more residues along a peptide chain. The upper table shows results for Pearson's correlation coefficients and the lower table does those for partial correlation coefficients. Significantly-positive correlation coefficients are found for almost all site pairs. In the phylogenetic trees of these protein families branch lengths are completely heterogeneous. The expected value of the probability of amino acid substitution in a branch is an increasing function of branch length;  $\Delta_{ib}^s \approx (1 - \exp(-\mu_i t_b))$  where  $\mu_i$  is an amino acid substitution rate for site  $i$ . Thus, Pearson's correlation coefficients of the expected values of substitution probability over branches between sites should be significantly positive, as shown in Table 2.

On the other hand, a partial correlation coefficient defined in Eq. 15 is a correlation coefficient between residuals that cannot be accounted for by a linear regression on the vectors of characteristic changes along branches at other sites. When dependences on other sites in the variation of substitutions are removed, significantly positive correlations ( $r > r_t$ ) are found only in a limited number of site pairs, and most site pairs show insignificant correlations. Furthermore, site pairs in the category of significantly-positive correlation tend to be contact residue site pairs with significantly-high probabilities; see the column of positive predictive value,  $PPV \equiv TP/(TP + FP)$ , where TP and FP are the numbers of true and false contact residue pairs, respectively. This result clearly indicates that the partial correlation coefficients represent the strength of the direct dependences of substitutions between sites.

## Co-evolution scores for site pairs

Concurrent substitutions between sites require that the direct correlation of substitutions must be positive. Therefore, only positive values of the partial correlation coefficients ( $\mathcal{C}_{ij}^s$ ) are used to define a co-evolution score ( $\rho_{ij}^s$ ) based on concurrent substitutions.

$$\rho_{ij}^s \equiv \max(\mathcal{C}_{ij}^s, 0) \quad (1)$$

For all other characteristic variables employed to detect co-evolving site pairs, the condition of concurrent substitutions between sites are a premise. Thus, instead of using partial correlations of characteristic variables themselves, the geometric mean of the partial correlation coefficient of each characteristic variable and the co-evolution score based on concurrent substitutions is used as a co-evolution score based on each characteristic change.

$$\rho_{ij}^x \equiv \text{sgn } \mathcal{C}_{ij}^x (|\rho_{ij}^s \mathcal{C}_{ij}^x|)^{1/2} \quad \text{for } x \in \{v, c, hb, h, \dots\} \quad (2)$$

As already mentioned in the Method section, negative correlations are required for characteristic variables such as volume, charge, and hydrogen bonding capacity to reflect compensatory substitutions.

In Table 3, TP and FP for each category of significantly positive ( $\rho_{ij}^x \geq r_t$ ) and negative ( $\rho_{ij}^x \leq -r_t$ ) correlations under the condition of  $|\rho_{ij}^x| \geq \rho_{ij}^s \geq r_t$  are listed for each characteristic variable. In the cases of volume, charge, and hydrogen bonding capacity, PPV for contact residue pairs is clearly larger in the category of significantly negative correlation than significantly positive correlation, indicating that these quantities to detect compensatory substitutions between sites are good predictors for close spatial proximity. Besides, there are more site pairs with significantly negative correlations than with significantly positive correlations, clearly indicating the presence of structural constraints against these physico-chemical changes.

To improve contact prediction by using characteristic variables  $\rho^x$  together with the characteristic variable  $\rho^s$  of concurrent substitutions, the PPV for the category of significantly positive or negative correlations should be larger than the PPV for concurrent substitutions. Both categories of significantly positive and negative correlations show better PPVs in the characteristic variables of hydrophobicity,  $\beta$  and turn propensities, aromatic interaction and branched side-chain. In the characteristic variables of cross-link capability and ionic side-chain, only the category of significantly positive correlation shows better PPV than the category of significantly positive correlation for concurrent substitutions. The  $\alpha$  propensity is not effective to detect contact residue pairs, although it may be effective to detect residue pairs within a helix or within helices. Based on these results, an overall co-evolution score for site pair  $(i, j)$  is defined here as

$$\begin{aligned} \rho_{ij} \equiv & \max[\rho_{ij}^s, \max(-\rho_{ij}^v, 0), \max(-\rho_{ij}^c, 0), \max(-\rho_{ij}^{hb}, 0), \\ & |\rho_{ij}^h|, |\rho_{ij}^\beta|, |\rho_{ij}^t|, |\rho_{ij}^{ar}|, |\rho_{ij}^{br}|, \max(\rho_{ij}^{cl}, 0), \max(\rho_{ij}^{ion}, 0)] \end{aligned} \quad (3)$$

## Contact prediction based on the overall co-evolution score $\rho_{ij}$

Co-evolving sites pairs are selected for contacts in the decreasing order of the overall co-evolution score  $\rho_{ij}$ . Although this score for co-evolution appears to be able to predict contact site pairs, preliminary results of contact prediction indicate that both terminal sites in multiple sequence alignments often have large values of  $\rho_{ij}^x$  ( $x \neq s$ ) for any other site, and also that there are a few sites showing extremely large values for  $\sum_j H(\rho_{ij} - r_t)$ ; the  $H$  denotes the Heaviside step function. Such an anomalous feature probably indicates a poor quality at these sites in multiple sequence alignments. Thus, in contact prediction,

1. the co-evolution scores of  $\rho_{ij}^x$  ( $x \neq s$ ) are ignored for both terminal sites in multiple sequence alignments; that is,  $\rho_{ij} \equiv \rho_{ij}^s$ .
2. Also, if  $\sum_j H(\rho_{ij} - r_t) > 15$ ,  $\rho_{ij} \equiv \rho_{ij}^s$  will be used for site  $i$ , and
3. if  $\sum_j H(\rho_{ij}^s - r_t) > 15$ ,  $\rho_{ij} \equiv 0$  will be used and such a site will be excluded in contact prediction.

The threshold value  $r_t$  used here is the value of correlation coefficient corresponding to E-value = 0.0001 in the Student's t-distribution. In the present contact prediction, only one site that is the N-terminal site in the multiple sequence alignment for the KH\_1 was excluded as an anomalous site.

Needless to say, the norm of any characteristic change vector is almost zero for invariant sites;  $\|\Delta_i\| \simeq 0$ . Therefore, invariant sites are excluded in the present method for contact prediction.

## Accuracy of contact site pairs predicted on the basis of the overall co-evolution score

Accuracies of predictions based on the overall co-evolution score and on the direct information (DI) score [26] calculated by a maximum entropy model are compared by using three measures in Table 4

for protein families listed in Table 1. Those three measures are PPV, mean Euclidean distance from predicted site pairs to the nearest true contact (MDPNT) in the 2-dimensional sequence-position space, and the mean Euclidean distance from every true contact to the nearest predicted site pair (MDTNP). The MDPNT and MDTNP, which were defined and used in [26], are qualitative measures of false positives and of the spread of predicted site pairs over true contacts, respectively. Smaller values of these measures indicate better predictions. For the predictions based on the DI score, the filters based on a secondary structure prediction and on disulfide bonds are not applied to the DI scores but only the filter [26] based on the degree of residue conservation at each site is, in order to compare the prediction accuracies of co-evolution and DI scores themselves.

The reliability of predicted co-evolving site pairs decreases with decreasing value of co-evolution score, and co-evolving site pairs are selected in the decreasing order of co-evolution score, therefore prediction accuracy tends to decrease as the total number of predicted sites pairs increases; see Fig. 2. In Table 4, the results of predictions in which the numbers of predicted contacts are equal to one fourth or one third of the number of true contacts are listed for each protein family. One third of the total number of true contacts is equal to the sequence length in the case of Trypsin, which has the largest number of contacts per residue, and equal to half of the sequence length in the case of Trans\_reg\_c and 7tm\_1, which have the smallest number of contacts per residue. This ratio was chosen, because Marks et al. [26] reported that one needs about 0.5 to 0.75 predicted distance constraints per residue or about 0.25 to 0.35 of the total number of contacts, to achieve reasonable three-dimensional structure prediction.

In Fig. 3 and Fig. S1, co-evolving site pairs are shown in the lower half of each triangular map in comparison with residue pairs whose minimum atomic distances are less than 5 Å. For comparison, contact residue pairs predicted with high DI scores [26] are also shown in the upper half of each triangular map. Gray filled-squares, red and indigo filled-circles indicate such residue-residue proximities, true and false positives in contact prediction, respectively. It should be noted here that residue pairs separated by 5 or fewer positions ( $|i - j| \leq 5$ ) in a sequence may be shown with the gray filled-squares but are excluded in the prediction of co-evolving site pairs and in the contact prediction with the DI score. The total number of predicted site pairs is equal to one third of the total number of true contacts in each protein structure.

In Table 4, which method is better in the accuracy of contact prediction is indicated by a bold font. The PPVs of the present method are comparable to or better than the DI method except CH, Kunitz\_BPTI, Lectin\_C, and RNase\_H. In Fig. 2, the PPVs of the present method and the DI method are drawn by solid and dotted lines as a function of the ratio of predicted to true contacts, respectively. Also, the values of MDPNT and of MDTNP are compared between the present and DI methods and also between the protein families in Figs. S2 and S3, respectively. The good performance of the present method is shown over a wide range of predicted site pairs.

## Dependence of the prediction accuracy on the number of predicted site pairs

The dependences of the accuracy of predicted contacts on their number are shown in Fig. 2 for PPV, in Fig. S2 for MDPNT, and in Fig. S3 for MDTNP. The total number of predicted site pairs takes every 10 from 10 to a sequence length; also accuracies for the numbers of predicted contacts equal to one third or one fourth of true contacts are plotted. Here, in order to compare prediction accuracies between protein families, the total number of predicted contacts is shown in the scale of the ratio of predicted to true contacts. It is clearly shown that there is an overall trend for PPV to decrease monotonically as increasing number of predicted site pairs. However, exceptional increases of PPV are also observed with increasing number of site pairs predicted. In the protein family of CH, PPV changes from 0.43 to 0.5 as the number of predicted site pairs increases from 30 to 50. Because except the case of CH such abnormal increases of PPV often occur in the range of small numbers of predicted site pairs, i.e., from 10 to 30, they may be caused by statistical fluctuations.



It is shown in Table 4 and Fig. S2 that the relationships of MDPNT with the ratio of predicted to true contacts are almost inverse of that of PPV, indicating that the MDPNT and PPV are two different measures of the quality of predicted site pairs but result in similar evaluations. On the other hand, MDTNP, which measures the spread of predicted site pairs over true contacts, differently measures the qualities of predicted contacts from PPV and MDPNT. It tends to decrease monotonically as the increasing number of predicted site pairs irrespective of the quality of prediction accuracy, and therefore it is not appropriate to measure the dependence of prediction accuracy on the total number of predicted site pairs.

## Dependence of the prediction accuracy on protein fold types

As expected, prediction accuracy is different between proteins. However, it is unexpected that prediction accuracy may be slightly lower for  $\alpha$  proteins, at least for the present three proteins, than for  $\beta$  proteins; see Fig. 2. Especially the prediction accuracy for the membrane protein 7tm\_1 is remarkably lower than other two  $\alpha$  proteins. This feature is observed in both the present and DI methods. Thus, this feature may originate in differences between structural constraints in  $\alpha$ - $\alpha$  packing and in packings of  $\beta$  strands and of  $\beta$  sheets, although the low prediction accuracy for the membrane protein 7tm\_1 would result from  $\alpha$ - $\alpha$  packing peculiar to membrane proteins. Here it should be noted that the  $\alpha$  proteins have less contacts per residue than the  $\beta$  proteins; see Table 4. A definitive answer must be postponed until more  $\alpha$  proteins are analyzed.

## Dependence of the prediction accuracy on the diversity and the number of sequences used

Multiple subsets of a full alignment are generated by using different values of threshold  $T_{bt}$  for branch length to remove OTUs connected to their parent nodes with short branches. In Fig. 4, Fig. S4, and Fig. S5, the PPVs, MDPNTs, and MDTNPs calculated from each data are plotted against the number of sequences used, respectively. Because the threshold values used to generate each dataset should also affect the accuracy of prediction, they are written near each data point. A general tendency is of course that the PPV and MDPNT are improved by using more sequences. However, the number of sequences and the threshold  $T_{bt}$  where accuracy improvement is saturated are very different between protein families. For example, in the case of SH3\_1, no significant improvement in the PPV and MDPNT is observed in a wide range of  $0.2 \geq T_{bt} \geq 0.001$ , even if the number of sequences increases from 1500 to 4000. In RNase\_H, the PPV and MDPNT are almost constant in the range of  $0.05 \geq T_{bt} \geq 0.001$  and  $2120 \leq n_{otu} \leq 7048$ . In Response\_reg, after the PPV reaches the highest value 0.73 at  $T_{bt} = 0.6$  and  $n_{otu} = 3344$ , it even decreases to 0.69 in  $3344 \leq n_{otu} \leq 7613$ , although its decrement is not large and the MDPNT is almost constant in this region. Multiple sequence alignments may include many sites where significant fraction of sequences have deletions, reducing effectively the number of sequences; for example, RNase\_H. However, it may be worth increasing the number of sequences until  $T_{bt} \approx 0.01$ . Here calculations have been carried out until  $n_{otu} \approx 7000$  or  $T_{bt} \approx 0.01$ . A few thousand sequences are necessary to get a reliable prediction for proteins consisting of a few hundred residues.

Some data points in Fig. 4, Fig. S4, and Fig. S5 correspond to datasets generated by using the same value of threshold but by removing different OTUs. PPV often differs between such datasets, although the difference of PPV ranges from a few percent to 8 percent; see the PPVs for  $T_{bt} = 0.2$  of Trans\_ref\_C,  $T_{bt} = 0.02$  of CH, and  $T_{bt} = 0.5$  of Cadherin in Fig. 4. This fact indicates that the distribution of sequences in a sequence space significantly affects prediction accuracy. Also, it is indicated that some site pairs predicted are still based on rare events of concurrent substitutions in a tree.

## Discussion

### Significance of compensatory substitutions in protein evolution

It has been shown that site pairs giving the significant values of partial correlation coefficients for substitutions, which concurrently occurred in branches of a phylogenetic tree and would be mostly compensatory substitutions, well correspond to contact site pairs in protein 3D structures. In compensatory substitutions, the fitness of first mutations must be negative, and successive mutations must occur to compensate the negative effect of the first mutation. A time scale in which compensatory mutations successively occur is much shorter than the time scale of protein evolution that is the order of fixation time for neutral mutations, otherwise negative mutants will be eliminated from a gene pool by selection. Thus, negative substitutions and their compensatory substitutions are expected to be observed as concurrent substitutions in the same branch of a tree. If substitutions are completely neutral, there will be no correlation in time when substitutions occur. Thus, a fact that contact site pairs can be well predicted by the present method indicates that compensatory substitutions are significant in protein evolution. Significance of compensatory substitutions was also indicated by a fact that likelihoods of phylogenetic trees can be significantly improved by taking account of codon substitutions with multiple nucleotide changes [29,30].

### Limitations in prediction accuracy

Prediction accuracy of contact residue pairs is different between the protein families. Possible reasons for false positives include (1) statistical noise due to an insufficient number of sequences, insufficient diversity of sequences, and incorrect matches in a multiple sequence alignment and an incorrect phylogenetic tree, (2) structural and functional constraints from other residues, which are not taken into account in the calculation of partial correlation coefficients from a correlation matrix, within a protein or even through other molecules involved in a molecular complex such as oligomerization, protein-substrate, and protein-DNA, (3) structural variance in homologous proteins, although each Pfam family is assumed to be iso-structural.

In reducing statistical noise, the diversity of sequences in protein families is more effective than the number of sequences itself. Also, the presence of many deletions in sequences reduces the value of including those sequences. The present subset ( $T_{bt} = 0.01$ ) of the full alignment of RNase\_H family consists of more than 4700 sequences, but their multiple sequence alignment includes many sites where the significant fraction of sequences have deletions. Here, branch lengths of sequences from their parent nodes in a phylogenetic tree are used to get less sequences but as diverse sequences as possible. Sequences whose branch lengths from their parent nodes are longer than 0.01 amino acid substitutions per site in a NJ tree are needed to be more than a few thousand, in order to get useful numbers ( $> 35\%$ ) of PPV. This requirement seems to be similar to that for the maximum entropy model [26], in which the order of one thousand sequences are required to reduce statistical noises including phylogenetic bias in frequency counts.

### Dependence on the accuracies of sequence alignment and phylogenetic tree

We do not extensively examine the dependence of contact prediction on the accuracy of phylogenetic tree. We tried to optimize a phylogenetic tree as well as model parameters for Kunitz\_BPTI, Lectin\_C, RNase\_H, and Response\_reg before evaluating characteristic variables at each site in each branch. The prediction accuracy of contact site pairs were not significantly improved. The improvement of prediction accuracy by a tree optimization from a NJ tree was within a few percent. The optimization of tree may be not cost-effective, because it requires a intensive calculation especially for thousands of sequences. An accurate multiple sequence alignment would be more critical to increase prediction accuracy.



In the present calculations, sites that are deletions in a target protein structure are excluded in the optimization of tree branches and in the calculation of partial correlation coefficients. The calculation of partial correlation coefficients by including those sites has been attempted for the Kunitz\_BPTI and RNase\_H domain families. No improvement was obtained at least for those protein families.

## A difference from methods of extracting residue type dependencies between sites

So far remarkable improvements in the accuracy of contact prediction were all achieved by extracting essential correlations of amino acid type between residue positions from multiple sequence alignments [23, 25–27]. Here, almost comparable accuracy of contact prediction has been achieved by evaluating direct correlations of concurrent and compensatory substitutions between sites. The present method cannot be applied to the cases in which all substitutions are nearly neutral. In such a case, structural and functional constraints from closely-located sites in protein 3D structures are reflected only in the joint distribution of amino acid types between the sites.

Residue-residue interactions maintaining secondary structures appear to be more easily detected by the joint distribution of amino acid types between the sites than concurrent substitutions. In general, the present method detects less dependences between neighboring sites along a sequence than the other. Marks et al. [26] reported that residue pairs separated by four or five positions in a sequence often have high DI scores without being in close physical proximity in the folded protein. Even for site pairs separated by more than five positions, their method based on the joint distribution of amino acid types detected more dependences in  $\alpha$  helical regions than the present method; see 7tm\_1 in Fig. 3.

From a such viewpoint, methods of extracting direct correlations of amino acid type between sites may be better for extracting direct dependences between sites than those of detecting compensatory substitutions in a tree. However, interactions between closely-located sites do not necessarily result in distinct correlations of amino acid type between the sites. For example, hydrophobic interactions are relatively non-specific, but significantly contribute to residue-residue interactions inside protein structures. The types of amino acids found inside protein structures are mainly hydrophobic. In the case of membrane proteins, most of amino acids embedded in membrane are hydrophobic. In the case that residue-residue interactions do not result in distinct correlations of amino acid type between sites, methods of detecting compensatory substitutions should perform better than methods of extracting direct correlations of amino acid type between sites. Membrane proteins may be this case; see 7tm\_1 in Fig. 2. Structural analyses of membrane proteins, especially the determinations of protein coordinates in transmembrane regions, are difficult in comparison of globular proteins. The present method for contact prediction could facilitate the coordinates determinations of membrane proteins.

Besides, the observed joint distributions of amino acid types include more or less phylogenetic bias as a statistical noise, but there is no such a noise in the present method. Thus, the both types of methods are complementary to each other.

## A difference between Bayesian graphical models and the present model

A Bayesian graphical model was applied to disentangling direct from indirect dependencies between residue positions in multiple sequence alignments of proteins [23]. In the Bayesian graphical model, an acyclic directed graph is assumed for site dependence, although interactions between sites in protein structures act on each other. A causal relationship between substitutions is of course directional. However, substitutions at a site affect on closely-located sites, and also the site is affected by substitutions at those surrounding sites. Thus, dependence between sites should be assumed to be bidirectional or undirectional. Unlike Bayesian graphical models, an undirected graph is assumed in a Gaussian graphical model [32], in which a null edge between two nodes encodes that random variables assigned to the nodes are conditionally independent of each other given the values of random variables assigned to other nodes. Assuming that

a joint probability density distribution of random variables is a multivariate Gaussian distribution, two random variables are conditionally independent given the values of other random variables if and only if a partial correlation coefficient between the two random variables is equal to zero. Thus, the present model based on partial correlation coefficients can be regarded as a Gaussian graphical model in which an undirected graph is assumed for dependences between sites and a feature vector  $\Delta_i$  is assigned to node  $i$  as the observed values of a random variable. This is one of essential differences between the present model and the Bayesian models [22–24], although there is another essential difference that the joint distributions of residues at sites were analyzed in [23, 24].

## Methods

### Mean of characteristic changes accompanied by substitutions at each site in each branch of a phylogenetic tree in a maximum likelihood model

Assuming that substitutions occur independently at each site, a likelihood  $P(\mathcal{A}|T, \Theta)$  of a sequence alignment  $\mathcal{A}$  in a phylogenetic tree  $T$  under a evolutionary model  $\Theta$  is represented as a product over sites of the likelihood of a sequence alignment  $\mathcal{A}_i$  for site  $i$ .

$$P(\mathcal{A}|T, \Theta) = \prod_i P(\mathcal{A}_i|T, \Theta) \quad (4)$$

$$P(\mathcal{A}_i|T, \Theta) = \sum_{\theta_\alpha} P(\mathcal{A}_i|T, \Theta, \theta_\alpha) P(\theta_\alpha) \quad (5)$$

where the distribution of  $\theta_\alpha$  for the variation of selective constraint [29, 30] are assumed to be *a priori* equal to  $P(\theta_\alpha)$ . The evolutionary model  $\Theta$  corresponds to a substitution model of amino acid or codon. Then, if substitutions are assumed to be in the equilibrium state of a time-reversible Markov process, the likelihood of a sequence alignment  $\mathcal{A}_i$  for site  $i$  will be calculated by taking any node as a root node. Let us assume here that the root node is a left node ( $v_{bL}$ ) of a branch  $b$ .

$$P(\mathcal{A}_i|T, \Theta, \theta_\alpha) = \sum_{\kappa} \sum_{\lambda} P(\mathcal{A}_i|v_{bL} = \kappa, v_{bR} = \lambda, T, \Theta, \theta_\alpha) \quad (6)$$

$$P(\mathcal{A}_i|v_{bL} = \kappa, v_{bR} = \lambda, T, \Theta, \theta_\alpha) \equiv \quad (7)$$

$$P_{bL}(\mathcal{A}_i|v_{bL} = \kappa, T, \Theta, \theta_\alpha) f_\kappa P(\lambda|\kappa, t_b, \Theta, \theta_\alpha) P_{bR}(\mathcal{A}_i|v_{bR} = \lambda, T, \Theta, \theta_\alpha) \quad (8)$$

where  $\kappa$  and  $\lambda$  indicate the type of codon or amino acid depending on the evolutionary model, and  $f_\kappa$  is the equilibrium frequency of  $\kappa$ .  $P(\lambda|\kappa, t_b, \Theta, \theta_\alpha)$  is a substitution probability from  $\kappa$  to  $\lambda$  at the branch  $b$  whose length is equal to  $t_b$ .  $P_{bL}(\mathcal{A}_i|v_{bL} = \kappa, T, \Theta, \theta_\alpha)$  is a conditional likelihood of the left subtree with  $v_{bL} = \kappa$  [33]. In the maximum likelihood (ML) method for phylogenetic trees, the tree  $T$  and parameters  $\Theta$  are estimated by maximizing the likelihood.

$$(\hat{T}, \hat{\Theta}) = \arg \max_{T, \Theta} P(\mathcal{A}|T, \Theta) \quad (9)$$

In this model, the mean  $\Delta_{ib}$  of a quantity  $\Delta_{\kappa\lambda}$  accompanied by substitutions from  $\kappa$  to  $\lambda$  at each site  $i$  in each branch  $b$  can be calculated as follows.

$$\Delta_{ib}(\mathcal{A}_i, \hat{T}, \hat{\Theta}, \theta_\alpha) \equiv \sum_{\kappa, \lambda} \frac{\Delta_{\kappa, \lambda} P(\mathcal{A}_i|v_{bL} = \kappa, v_{bR} = \lambda, \hat{T}, \hat{\Theta}, \theta_\alpha)}{P(\mathcal{A}_i|\hat{T}, \hat{\Theta}, \theta_\alpha)} \quad (10)$$

$$\Delta_{ib}(\mathcal{A}_i, \hat{T}, \hat{\Theta}) = \sum_{\theta_\alpha} \Delta_{ib}(\mathcal{A}_i, \hat{T}, \hat{\Theta}, \theta_\alpha) P(\theta_\alpha|\mathcal{A}_i, \hat{T}, \hat{\Theta}) \quad (11)$$

where  $P(\theta_\alpha|\mathcal{A}_i, \hat{T}, \hat{\Theta})$  is a posterior probability calculated from

$$P(\theta_\alpha|\mathcal{A}_i, \hat{T}, \hat{\Theta}) = \frac{P(\mathcal{A}_i|\hat{T}, \hat{\Theta}, \theta_\alpha)P(\theta_\alpha)}{P(\mathcal{A}_i|\hat{T}, \hat{\Theta})} \quad (12)$$

If  $\Delta_{\kappa\lambda}$  is defined to be equal to 1 for  $\kappa \neq \lambda$  and 0 for  $\kappa = \lambda$ ,  $\Delta_{ib}(\mathcal{A}_i, \hat{T}, \hat{\Theta})$  will represent the expected value of substitution probability at site  $i$  in branch  $b$ . Let us define a vector  $\Delta_i$  as follows, and consider the correlation of the two vectors,  $\Delta_i$  and  $\Delta_j$ .

$$\Delta_i \equiv (\dots, \Delta_{ib}(\mathcal{A}_i, \hat{T}, \hat{\Theta}) - \frac{\sum_b \Delta_{ib}(\mathcal{A}_i, \hat{T}, \hat{\Theta})}{\sum_b 1}, \dots)' \quad (13)$$

where  $'$  denotes the transpose of a matrix. A correlation matrix  $C$  is defined to be a matrix whose  $(i, j)$  element is the correlation coefficient  $r_{\Delta_i \Delta_j}$  between  $\Delta_i$  and  $\Delta_j$ .

$$C_{ij} \equiv r_{\Delta_i \Delta_j} = \frac{(\Delta_i, \Delta_j)}{\|\Delta_i\| \|\Delta_j\|} \quad (14)$$

where  $(\Delta_i, \Delta_j)$  denotes the inner product of the two vectors. The correlation between sites  $i$  and  $j$  may be an indirect correlation resulting from correlations between sites  $i$  and  $k$  and between sites  $k$  and  $j$ . To remove such indirect correlations, partial correlation coefficients are used here. The partial correlation coefficient is a correlation coefficient between residual vectors ( $\Pi_{\perp\{\Delta_{k \neq i, j}\}}\Delta_i$  and  $\Pi_{\perp\{\Delta_{k \neq i, j}\}}\Delta_j$ ) of given two vectors that are perpendicular to a subspace consisting of other vectors except those two vectors ( $\Delta_i$  and  $\Delta_j$ ) and therefore cannot be accounted for by a linear regression on other vectors;  $\Pi_{\perp\{\Delta_{k \neq i, j}\}}$  is a projection operator to a space perpendicular to the subspace. If the correlation matrix is regular, then the partial correlation coefficients  $\mathcal{C}_{ij}$  will be related to the  $(i, j)$  element of its inverse matrix.

$$\mathcal{C}_{ij} \equiv r_{\Pi_{\perp\{\Delta_{k \neq i, j}\}}\Delta_i \Pi_{\perp\{\Delta_{k \neq i, j}\}}\Delta_j} = \frac{(\Pi_{\perp\{\Delta_{k \neq i, j}\}}\Delta_i, \Pi_{\perp\{\Delta_{k \neq i, j}\}}\Delta_j)}{\|\Pi_{\perp\{\Delta_{k \neq i, j}\}}\Delta_i\| \|\Pi_{\perp\{\Delta_{k \neq i, j}\}}\Delta_j\|} = - \frac{(C^{-1})_{ij}}{((C^{-1})_{jj}(C^{-1})_{ii})^{1/2}} \quad (15)$$

## Characteristic variables indicating co-evolution between sites

The following characteristic changes accompanied by substitutions whose correlations indicate co-evolution between sites have been used here.

1. Occurrence of amino acid substitution.

The most primary quantity is one ( $\Delta^s$ ) that is defined as follows and indicates the occurrence of amino acid substitution at a site.

$$\Delta_{\kappa, \lambda}^s \equiv 1 - \delta_{a_\kappa, a_\lambda} \quad (16)$$

where  $\delta_{a_\kappa, a_\lambda}$  is the Kronecker's  $\delta$  that takes 1 if  $a_\kappa = a_\lambda$  and 0 otherwise. The  $a_\kappa$  is the type of amino acid corresponding to  $\kappa$ .  $\Delta_{ib}^s(\mathcal{A}_i, \hat{T}, \hat{\Theta})$  in Eq. 11 indicates the expected value of the probability of amino acid substitution at site  $i$  in branch  $b$ . This quantity was also used [7, 22] for the prediction of contact residue pairs in protein structures.

2. Volume change of a side chain accompanied by an amino acid substitution.

Protein structures must be tightly packed [34], and therefore mutations between amino acids whose side chain volumes significantly differ tend to unstabilize protein structures and therefore will be

eliminated from a gene pool by selection [35] unless the volume change is compensated by successive mutations at sites closely located in protein structures. Thus, the volume changes of side chains caused by amino acid substitutions are used to detect co-evolution between closely located sites in protein structures.

$$\Delta_{\kappa,\lambda}^v \equiv \text{side\_chain\_volume}_{a_\lambda} - \text{side\_chain\_volume}_{a_\kappa} \quad (17)$$

where  $\text{side\_chain\_volume}_{a_\lambda}$  means the volume of side chain  $a_\lambda$ . The amino acid volumes used here are the mean volume occupied by each type of amino acid in protein structures, and taken from the set named BL+ in Table 6 of [36]; the volume of a half cystine (labeled as "cys" in the table) is used here for a cysteine.

3. Charge change of a side chain accompanied by an amino acid substitution.

Charge-charge interactions in protein structures are known to be significant. Substitutions that keep favorable charge-charge interactions are expected to be advantageous in selection.

$$\Delta_{\kappa,\lambda}^c \equiv \text{side\_chain\_charge}_{a_\lambda} - \text{side\_chain\_charge}_{a_\kappa} \quad (18)$$

where  $\text{side\_chain\_charge}_{a_\kappa}$  represents a charge of side chain type  $a_\kappa$  and takes 1 for positively charged side chains (arg and lys), 0.1 for his, and  $-1$  for negatively charged ones (asp, glu).

4. Change of hydrogen-bonding capability accompanied by an amino acid substitution.

One of the most important interactions to stabilize protein structures is a hydrogen-bonding interaction. Substitutions that keep hydrogen-bonds are favorable. In order to detect whether hydrogen-bonds between side chains can be kept despite substitutions, the change of hydrogen-bonding capability is defined here as

$$\Delta_{\kappa,\lambda}^{hb} \equiv \text{acceptor\_capability}_{a_\lambda} - \text{acceptor\_capability}_{a_\kappa} + /nonumber \quad (19)$$

$$\text{donor\_capability}_{a_\lambda} - \text{donor\_capability}_{a_\kappa} \quad (20)$$

where  $\text{acceptor\_capability}_{a_\kappa}$  takes  $-1$  if a side chain  $a_\kappa$  can be an hydrogen-bonding acceptor and 0 otherwise.  $\text{Donor\_capability}_{a_\lambda}$  takes 1 if a side chain  $a_\lambda$  can be a hydrogen-bonding donor and 0 otherwise. Hydrogen-bonding acceptors are asn, asp, gln, glu, his, ser, thr, and tyr. Hydrogen-bonding donors are arg, asn, gln, his, lys, ser, thr, trp, and tyr. A negative correlation is expected for this quantity between closely located sites in a protein 3D structure.

5. Change of hydrophobicity accompanied by an amino acid substitution

Also, hydrophobic interactions are crucial for a polypeptide chain to be folded into a unique three-dimensional structure. Hydrophobic interactions may be correlated between substitutions at nearby sites in a protein 3D structure.

$$\Delta_{\kappa,\lambda}^h \equiv e_{a_\lambda r} - e_{a_\kappa r} \quad (21)$$

where  $e_{a_\kappa r}$  is the mean contact energy of an amino acid  $a_\kappa$  with surrounding residues ( $r$ ) in protein structures; see [37] for its exact definition.

6. Changes of  $\beta$  and turn propensities accompanied by an amino acid substitution.

Changes of  $\beta$  and turn propensities [38] are also examined.

$$\Delta_{\kappa,\lambda}^\beta \equiv \beta\_sheet\_propensity_{a_\lambda} - \beta\_sheet\_propensity_{a_\kappa} \quad (22)$$

$$\Delta_{\kappa,\lambda}^t \equiv \text{turn\_propensity}_{a_\lambda} - \text{turn\_propensity}_{a_\kappa} \quad (23)$$

where  $\beta\_sheet\_propensity_{a_\kappa}$  is the value of  $\beta$  sheet propensity [38] of amino acid  $a_\kappa$ . The change of  $\alpha$  propensity is also examined but it is not used as a co-evolution score.

7. Change of the capability of aromatic interaction accompanied by an amino acid substitution.

$$\Delta_{\kappa,\lambda}^{ar} \equiv \delta_{\text{aromatic\_side\_chains},a_\lambda} - \delta_{\text{aromatic\_side\_chains},a_\kappa} \quad (24)$$

where  $\delta_{\text{aromatic\_side\_chains},a_\kappa}$  is equal to 1 if  $a_\kappa$  is one of aromatic side-chains (his, phe, trp, and tyr) and 0 otherwise.

8. Change of branched side-chain accompanied by an amino acid substitution.

$$\Delta_{\kappa,\lambda}^{br} \equiv \delta_{\text{aliphatic\_branched\_side\_chains},a_\lambda} - \delta_{\text{aliphatic\_branched\_side\_chains},a_\kappa} \quad (25)$$

where  $\delta_{\text{aliphatic\_branched\_side\_chains},a_\kappa}$  is equal to 1 if  $a_\kappa$  is one of aliphatic branched side-chains (ile, leu and val), and 0 otherwise.

9. Change of cross-link capability accompanied by an amino acid substitution.

$$\Delta_{\kappa,\lambda}^{cl} \equiv \delta_{\text{cross\_link},a_\lambda} - \delta_{\text{cross\_link},a_\kappa} \quad (26)$$

where  $\delta_{\text{cross\_link},a_\kappa}$  is equal to 1 if  $a_\kappa$  is one of asn, gln, ser and thr, and 0 otherwise.

10. Change of ionic side-chain accompanied by an amino acid substitution.

$$\Delta_{\kappa,\lambda}^{ion} \equiv \delta_{\text{ionic\_side\_chains},a_\lambda} - \delta_{\text{ionic\_side\_chains},a_\kappa} \quad (27)$$

where  $\delta_{\text{ionic\_side\_chains},a_\kappa}$  is equal to 1 if  $a_\kappa$  is one of ionic side-chains (asp, glu, arg, and lys), 0.1 if  $a_\kappa$  is his, and 0 otherwise.

## A mechanistic codon substitution model for the maximum likelihood inference of phylogenetic tree

A mechanistic codon substitution model, in which each codon substitution rate is proportional to the product of a codon mutation rate and the average fixation probability depending on the type of amino acid replacement, has advantages [29, 30] over nucleotide, amino acid, and empirical codon substitution models in evolutionary analysis of protein-coding sequences, because mutation at the nucleotide level and selection at the amino acid level can be separately evaluated. Even for amino acid sequences of OTUs (operational taxonomic units), the mechanistic codon substitution model with the prior assumption of equal codon usage for them yields smaller AIC values (Akaike Information Criterion) than any amino acid substitution model does (unpublished). Thus, the mechanistic codon substitution model [30] is used here to evaluate the likelihood of a phylogenetic tree and the posterior means of characteristic variables at each site in each branch.

In the mechanistic codon substitution model, in which substitutions are assumed to be in the stationary state of a time-homogeneous reversible Markov process, the substitution probability matrix in time  $t$  is represented as  $\exp Rt$  with a substitution rate matrix  $R$ , which is defined as

$$R_{\mu\nu} = C_{\text{const}} M_{\mu\nu} \frac{f_\nu}{f_{\text{mut}}} e^{w_{\mu\nu}} \text{ for } \mu \neq \nu \quad (28)$$

where  $M_{\mu\nu}$  is the mutation rate from codon  $\mu$  to  $\nu$ ,  $f_{\nu}^{\text{mut}}$  is the equilibrium frequency of codon  $\nu$  in nucleotide mutations,  $f_{\nu}$  is the equilibrium codon frequency,  $\frac{f_{\nu}}{f_{\nu}^{\text{mut}}}e^{w_{\mu\nu}}$  is the average rate of fixation, and  $w_{\mu\nu}$  is the selective constraints for mutations from  $\mu$  to  $\nu$ ; refer to [30] for details. Assuming that nucleotide mutations occur independently at each codon position but multiple nucleotide mutations in a codon can instantaneously occur, the mutation rate matrix  $M$  is approximated with 9 parameters; the ratios of nucleotide mutation rates,  $m_{tc|ag}/m_{[tc][ag]}$ ,  $m_{ag}/m_{tc|ag}$ ,  $m_{ta}/m_{[tc][ag]}$ ,  $m_{tg}/m_{[tc][ag]}$ , and  $m_{ca}/m_{[tc][ag]}$ , the relative ratio  $m$  of multiple nucleotide changes, and the equilibrium nucleotide frequencies in nucleotide mutations,  $f_a^{\text{mut}}$ ,  $f_c^{\text{mut}}$ , and  $f_g^{\text{mut}}$ . The selective constraint  $w_{\mu\nu}$  for a protein family is approximated with a linear function of the mean selective constraints that were evaluated [29] by ML-fitting a substitution matrix based on the mechanistic codon model to an empirical amino acid substitution matrix. Here we use the mean selective constraints  $w_{\mu\nu}^{\text{LG}}$  derived from the empirical amino acid substitution matrix LG [39]. The slope  $\beta$  and a constant term  $w_0$  are parameters;  $w_{\mu\nu} = \beta w_{\mu\nu}^{\text{LG}} + w_0$ . The selective constraint  $w_{\mu\nu}$  is assumed to vary across sites and the variation of selective constraints [30] has been approximated by a discrete gamma distribution [31] with 4 categories. Thus, one more parameter is a shape parameter  $\alpha$  for the discrete gamma distribution. In the result, 12 parameters in addition to the equilibrium frequencies of codons must be determined in this model. See [30] for full details of these parameters.

The equilibrium frequencies of codons are estimated to be equal to codon frequencies in sequences of OTUs with the assumption of equal codon usage for amino acid sequences. Other 12 parameters were estimated by maximizing the likelihood of a NJ tree of Pfam seed sequences. Then, the ML estimates of the parameters obtained from the Pfam seed sequences are used to evaluate branch lengths and posterior means of characteristic variables at each site in each branch of NJ trees for the subsets of Pfam full alignments. NJ trees taken from the Pfam were used for the tree topologies, because optimizing tree topologies for more than a few thousands of sequences require too much computational time. Branch optimization of phylogenetic trees and posterior means of characteristic variables are calculated using Phym [40] modified for the mechanistic codon substitution model.

## Definition of contact residue pairs in protein structures

Contact residue pairs are arbitrarily defined here as residue pairs whose minimum atomic distances are shorter than 5 Å and which are separated by 6 or more residues along a peptide chain. This definition, especially the latter condition, which was used in Marks et al. [26] is employed here only for the comparison of the present predictions with their predictions of contact residue pairs.

The PDB ID of a protein structure used for a target protein in each Pfam family is listed in Table 1. The amino acid sequences of these PDB entries are just the same as those of the Uniprot IDs, which are also listed in Table 1.



## Acknowledgments

## References

1. Yanovsky C, Horn V, Thorpe D (1964) Protein structure relationships revealed by mutation analysis. *Science* 146: 1593-1594.
2. Fitch WM, Markowitz E (1970) An improved method for determining codon variability in a gene and its application to the rate of fixation of mutations in evolution. *Biochem Genet* 4: 579-593.
3. Bazykin G, Kondrashov F, Ogurtsov A, Sunyaev S, Kondrashov A (2004) Positive selection at sites of multiple amino acid replacements since rat-mouse divergence. *Nature* 429: 558-562.
4. Maisnier-Patin S, Andersson DI (2004) Adaptation to the deleterious effect of antimicrobial drug resistance mutations by compensatory evolution. *Research in Microbiology* 155: 360-369.
5. Altschuh D, Vernet T, Berti P, Moras D, Nagai K (1988) Coordinated amino acid changes in homologous protein families. *Protein Eng* 2: 193-199.
6. Göbel U, Sander C, Schneider R, A V (1994) Correlated mutations and residue contacts in proteins. *Proteins* 18: 309-317.
7. Shindyalov IN, Kolchanov NA, Sander C (1994) Can three-dimensional contacts in protein structures be predicted by analysis of correlated mutations? *Protein Eng* 7: 349-358.
8. Pollock DD, Taylor WR (1997) Effectiveness of correlation analysis in identifying protein residues undergoing correlated evolution. *Protein Eng* 10: 647-657.
9. Pollock DD, Taylor WR, Goldman N (1999) Coevolving protein residues: maximum likelihood identification and relationship to structure. *J Mol Biol* 287: 187-198.
10. Atchley WR, Wollenberg KR, Fitch WM, Terhalle W, Dress AW (2000) Correlations among amino acid sites in bhlh protein domains: an information theoretic analysis. *Mol Biol Evol* 17: 164-178.
11. Fariselli P, Olmea O, Valencia A, Casadio R (2001) Prediction of contact maps with neural networks and correlated mutations. *Protein Eng* 14: 835-843.
12. Fodor AA, Aldrich RW (2004) Influence of conservation on calculations of amino acid covariance in multiple sequence alignment. *Proteins* 56: 211-221.
13. Martin LC, Gloor GB, Dunn SD, Wahl LM (2005) Using information theory to search for co-evolving residues in proteins. *Bioinformatics* 21: 4116-4124.
14. Fares M, Travers S (2006) A novel method for detecting intramolecular coevolution. *Genetics* 173: 9-23.
15. Gouveia-Oliveira R, Pedersen A (2007) Finding coevolving amino acid residues using row and column weighting of mutual information and multi-dimensional amino acid representation. *Algorithms for Molecular Biology* 2: 12.
16. Dunn SD, Wahl LM, Gloor GB (2008) Mutual information without the influence of phylogeny or entropy dramatically improves residue contact prediction. *Bioinformatics* 24: 333-340.
17. Skerker JM, Perchuk BS, Siryaporn A, Lubin EA, Ashenberg O, et al. (2008) Rewiring the specificity of two-component signal transduction systems. *Cell* 133: 1043-1054.

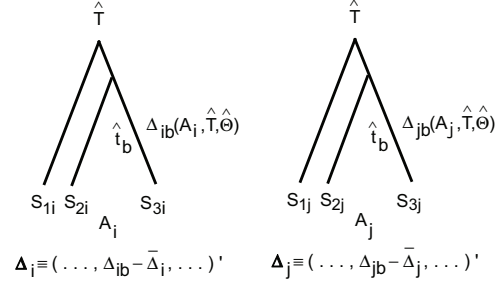
18. Weigt M, White RA, Szurmant H, Hoch JA, Hwa T (2009) Identification of direct residue contacts in protein-protein interaction by message passing. *Proc Natl Acad Sci USA* 106: 67-72.
19. Lockless SW, Ranganathan R (1999) Evolutionarily conserved pathways of energetic connectivity in protein families. *Science* 8: 295-299.
20. Yeang CH, Haussler D (2007) Detecting coevolution in and among protein domains. *PLoS Computational Biology* 3: e211.
21. Punta M, Coggill PC, Eberhardt RY, Mistry J, Tate J, et al. (2012) The pfam protein families database. *Nucl Acid Res* 40: D290-D301.
22. Poon AFY, Lewis FI, Frost SDW, Kosakovsky Pond SL (2008) Spidermonkey: rapid detection of co-evolving sites using bayesian graphical models. *Bioinformatics* 24: 1949-1950.
23. Burger L, van Nimwegen E (2008) Accurate prediction of protein-protein interactions from sequence alignments using a bayesian method. *Mol Syst Biol* 4: 165.
24. Burger L, van Nimwegen E (2010) Disentangling direct from indirect co-evolution of residues in protein alignments. *PLoS Comp Biol* 6: e1000633.
25. Morcos F, Pagnani ALB, Bertolind A, Marks DS, Sander C, et al. (2011) Direct-coupling analysis of residue coevolution captures native contacts across many protein families. *Proc Natl Acad Sci USA* 108: E1293-E1301.
26. Marks DS, Colwell LJ, Sheridan R, Hopf TA, Pagnani A, et al. (2011) Protein 3d structure computed from evolutionary sequence variation. *PLoS One* 6: e28766.
27. Taylor WR, Sadowski MI (2011) Structural constraints on the covariance matrix derived from multiple aligned protein sequences. *PLoS ONE* 6: e28265.
28. Saitou N, Nei M (1987) The neighbor-joining method: A new method for reconstructing phylogenetic trees. *MolBiolEvol* 4: 406-425.
29. Miyazawa S (2011) Selective constraints on amino acids estimated by a mechanistic codon substitution model with multiple nucleotide changes. *PLoS One* 6: e17244.
30. Miyazawa S (2011) Advantages of a mechanistic codon substitution model for evolutionary analysis of protein-coding sequences. *PLoS One* 6: e28892.
31. Yang Z (1994) Maximum likelihood phylogenetic estimation from dna sequences with variable rates over sites: approximate methods. *J Mol Evol* 39: 306-314.
32. Edward D (2000) Introduction to graphical modelling. New York: Springer.
33. Felsenstein J (1981) Evolutionary trees from dna sequences: A maximum likelihood approach. *J Mol Evol* 17: 368-376.
34. Richards FM (1977) Area, volumes, packing, and protein structure. *Annu Rev Biophys Bioeng* 6: 151-176.
35. Go M, Miyazawa S (1978) Volume and polarity changes accompanied by amino acid substitutions in protein evolution. *International Journal of Peptide and Protein Research* 12: 237- 241.
36. Tsai J, Taylor R, Chothia C, Gerstein M (1999) The packing density in proteins: standard radii and volumes. *J Mol Biol* 290: 253-266.

37. Miyazawa S, Jernigan RL (1996) Residue-residue potentials with a favorable contact pair term and an unfavorable high packing density term for simulation and threading. *J Mol Biol* 256: 623-644.
38. Chou PY, Fasman FD (1978) Prediction of the secondary structure of proteins from their amino acid sequence. *J Adv Enzymol* 47: 45-148.
39. Le SQ, Gascuel O (2008) An improved general amino acid replacement matrix. *Mol Biol Evol* 25: 1307-1320.
40. Guindon S, Gascuel O (2003) Simple, fast, and accurate algorithm to estimate large phylogenies by maximum likelihood. *Syst Biol* 52: 696-704.

## Figure Legends

**Topology:** by the Neighbor joining method

**Branch lengths:** by a ML method in a mechanistic codon substitution model



**Correlation coefficient matrix of feature vectors between sites:**

$$(C)_{ij} \equiv r_{\Delta_i \Delta_j} = \frac{(\Delta_i, \Delta_j)}{\|\Delta_i\| \|\Delta_j\|}$$

**Partial correlation coefficients of feature vectors between sites:**

$$\mathcal{C}_{ij} \equiv \frac{(\Pi_{\perp\{\Delta_{k \neq i,j}\}} \Delta_i, \Pi_{\perp\{\Delta_{k \neq i,j}\}} \Delta_j)}{\|\Pi_{\perp\{\Delta_{k \neq i,j}\}} \Delta_i\| \|\Pi_{\perp\{\Delta_{k \neq i,j}\}} \Delta_j\|} = - \frac{(C^{-1})_{ij}}{((C^{-1})_{ii}(C^{-1})_{jj})^{1/2}}$$

**Co-evolution score based on partial correlation coefficients:**

$$\rho_{ij} \equiv \max[\rho_{ij}^s, \max(-\rho_{ij}^v, 0), \max(-\rho_{ij}^c, 0), \max(-\rho_{ij}^{hb}, 0), |\rho_{ij}^h|, \dots]$$

$$\rho_{ij}^s \equiv \max(\mathcal{C}_{ij}^s, 0), \rho_{ij}^x \equiv \text{sgn } \mathcal{C}_{ij}^x (|\rho_{ij}^s \mathcal{C}_{ij}^x|)^{1/2} \quad (x \in \{v, c, hb, h, \dots\})$$

**Figure 1. Framework of the present model.** See text for details.

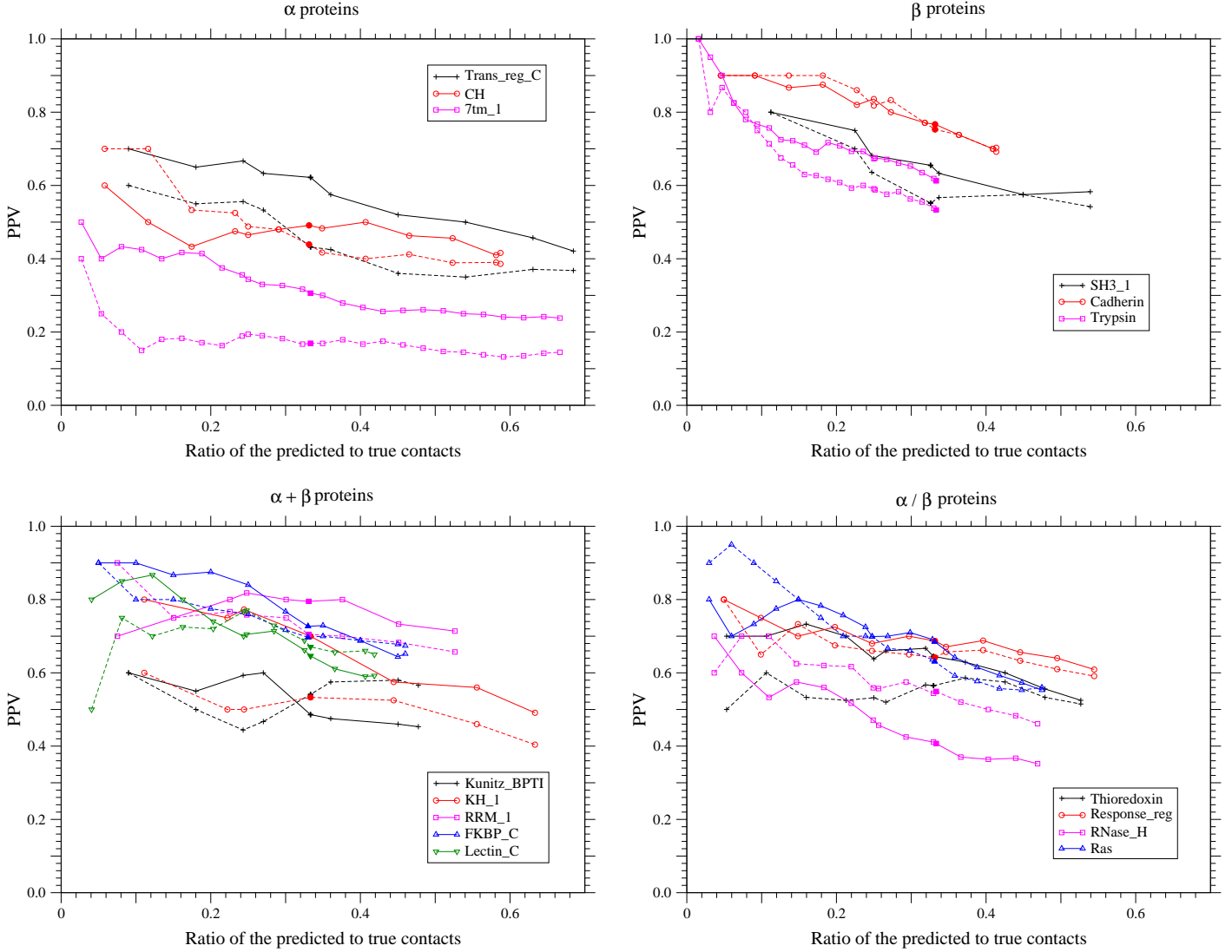


**Figure 2. Dependence of PPV on the number of predicted contacts.** The dependences of the positive predictive values on the total number of predicted contacts are shown for each protein fold of  $\alpha$ ,  $\beta$ ,  $\alpha + \beta$ , and  $\alpha / \beta$ . The solid and dotted lines show the PPVs of the present method and the method based on the DI score [26], respectively. The total number of predicted site pairs is shown in the scale of the ratio of the number of predicted site pairs to the number of true contacts. The total number of predicted site pairs takes every 10 from 10 to a sequence length; also PPVs for the numbers of predicted site pairs equal to one fourth or one third of true contacts are plotted. The filled marks indicate the points corresponding to the number of predicted site pairs equal to one third of the number of true contacts. The number of sequences used here for each protein family is one listed in Table 1.

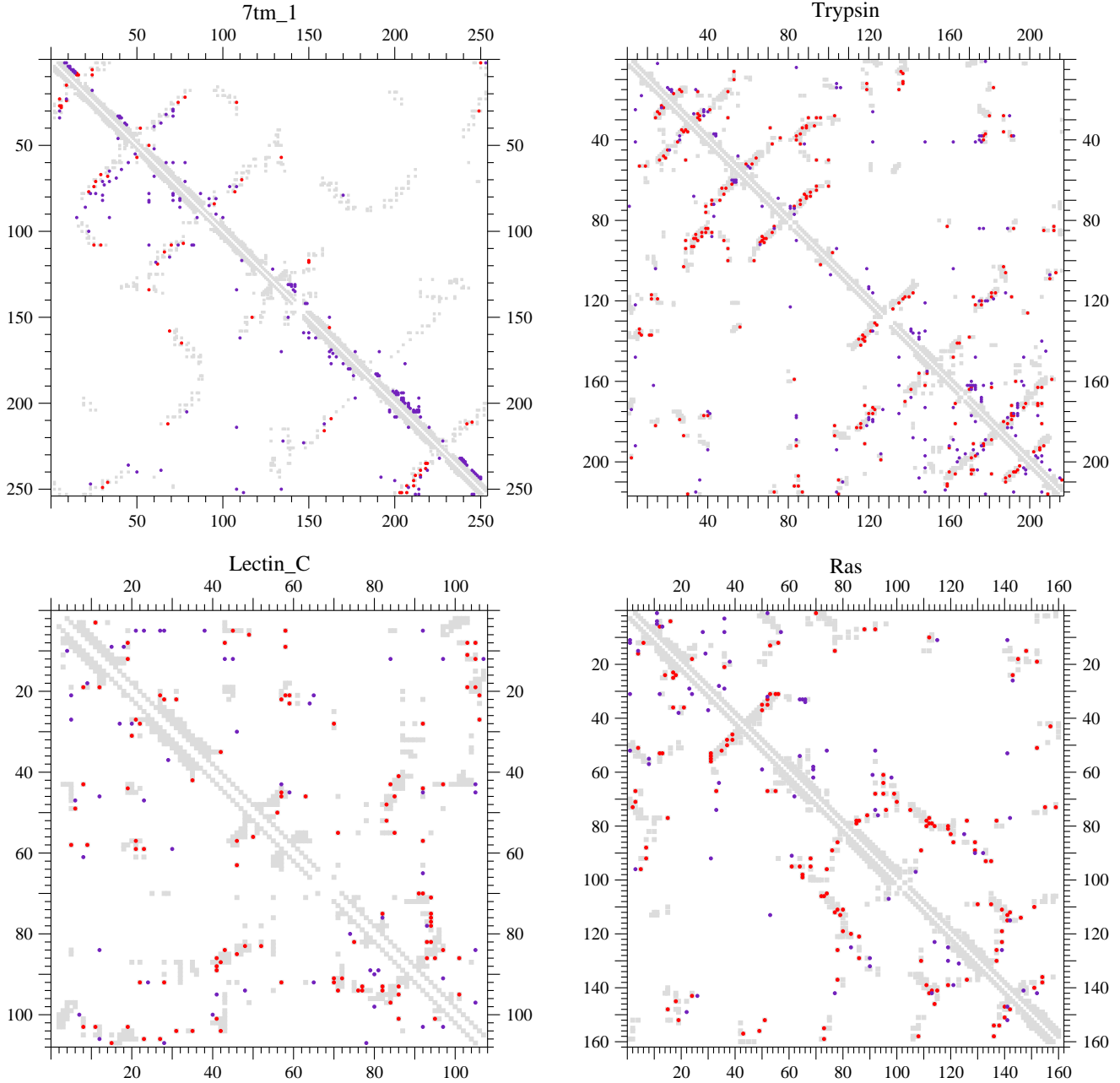


**Figure 3. Co-evolving site pairs versus DI residue pairs.** Residue pairs whose minimum atomic distances are shorter than 5 Å in a protein structure and co-evolving site pairs predicted are shown by gray filled-squares and by red or indigo filled-circles in the lower-left half of each figure, respectively. For comparison, such residue-residue proximities and predicted contact residue pairs with high DI scores in [26] are also shown by gray filled-squares and by red or indigo filled-circles in the upper-right half of each figure, respectively; only the conservation filter is applied but the filters based on a secondary structure prediction and for cysteine pairs are not applied to the DI scores. Red and indigo filled-circles correspond to true and false contact residue pairs, respectively. Residue pairs separated by five or fewer positions in a sequence may be shown with the gray filled-squares but are excluded in both the predictions. The total numbers of co-evolving site pairs and DI residue pairs plotted for each protein are both equal to one third of true contacts ( $TP + FP = \#contacts/3$ ). The PPVs of both the methods for each protein are listed in Table 4.



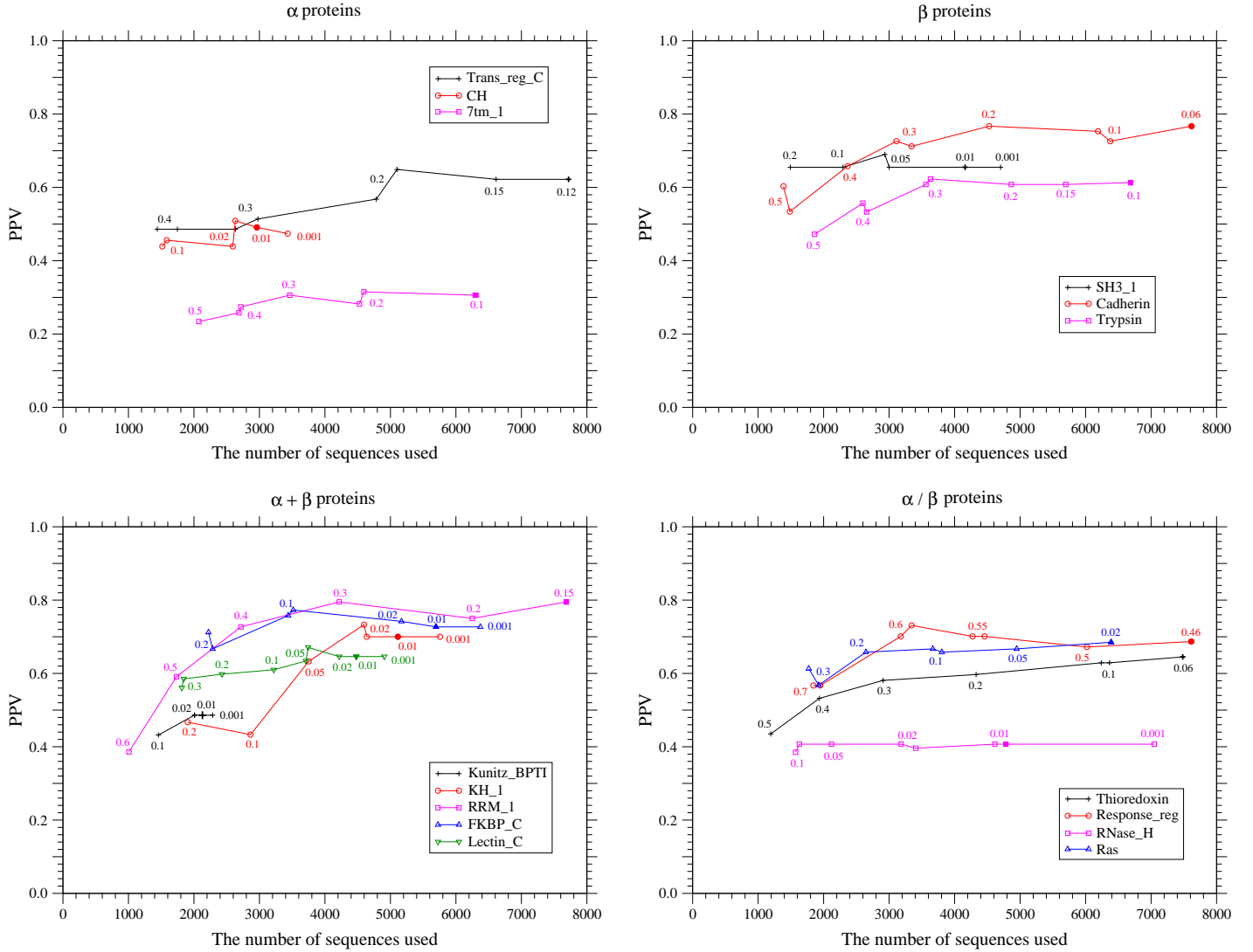


**Figure 4. Dependence of PPV on the number of sequences used.** The positive predictive values are plotted against the total number of homologous sequences used for each prediction. The filled marks indicate the points corresponding to the number of used sequences listed for each protein family in Table 1. The values written near each data point indicate the threshold value  $T_{bt}$ ; OTUs connected to their parent nodes with branches shorter than this threshold value are removed in the NJ tree of the Pfam full sequences used for each prediction. Some data points correspond to datasets generated by using the same value of the threshold but by removing different OTUs.

## Tables

**Table 1. Protein families used.**

Pfam ID <sup>a</sup>	Seed <sup>b</sup>	Full <sup>c</sup>	Target protein domain		Fold type	No. sites/Length <sup>f</sup>
			Uniprot ID <sup>d</sup>	PDB ID <sup>e</sup>		
Trans_reg_C	362	35180	OMPR_ECOLI/156-232	1ODD-A:156-232	$\alpha$	76/77
CH	202	5756	SPTB2_HUMAN/176-278	1BKR-A:5-107	$\alpha$	101/103
7tm_1	64	26656	OPSD_BOVIN/54-306	1GZM-A:54-306	$\alpha$ (tm) <sup>g</sup>	248/253
SH3_1	61	8993	YES_HUMAN/97-144	2HDA-A:97-144	$\beta$	48/48
Cadherin	57	18808	CADH1_HUMAN/267-366	2O72-A:113-212	$\beta$	91/100
Trypsin	71	14720	TRY2_RAT/24-239	3TGI-E:16-238	$\beta$	212/216
Kunitz_BPTI	151	3090	BPT1_BOVIN/39-91	5PTI-A:4-56	$\alpha + \beta$	53/53
KH_1	399	11484	PCBP1_HUMAN/281-343	1WVN-A:7-69	$\alpha + \beta$	57/63
RRM_1	79	31837	ELAV4_HUMAN/48-118	1G2E-A:41-111	$\alpha + \beta$	70/71
FKBP_C	174	11034	O45418_CAEEL/26-118	1R9H-A:26-118	$\alpha + \beta$	92/93
Lectin_C	44	6530	CD209_HUMAN/273-379	1SL5-A:273-379	$\alpha + \beta$	103/107
Thioredoxin	50	16281	THIO_ALIAC/1-103	1RQM-A:1-103	$\alpha/\beta$	99/103
Response_reg	57	103232	CHEY_ECOLI/8-121	1E6K-A:8-121	$\alpha/\beta$	110/114
RNase_H	65	13801	RNH_ECOLI/2-142	1F21-A:3-142	$\alpha/\beta$	128/140
Ras	61	13525	RASH_HUMAN/5-165	5P21-A:5-165	$\alpha/\beta$	159/161

<sup>a</sup> Pfam release 26.0 (November 2011) was used.

<sup>b</sup> The number of sequences included in the seed alignment of the Pfam.

<sup>c</sup> The number of sequences included in the full alignment of the Pfam.

<sup>d</sup> Target protein domain in the Pfam family.

<sup>e</sup> A protein structure corresponding to the target protein domain.

<sup>f</sup> Unreliable site positions that are represented by the lower case of characters in alignments were excluded in the evaluation of prediction accuracy.

<sup>g</sup> Transmembrane  $\alpha$ .

**Table 2.** Correlation ( $r_{\Delta_i^s \Delta_j^s}$ ) versus partial correlation ( $r_{\Pi_{\perp} \Delta_i^s \Pi_{\perp} \Delta_j^s}$ ) coefficients of concurrent substitutions between sites.

Pfam ID	$T_{bt}^a$	#seqs <sup>a</sup>	$C_{ij}^s \geq r_t^b$		$r_t > C_{ij}^s > 0$		$0 > C_{ij}^s > -r_t$		$-r_t \geq C_{ij}^s$	
			TP:FP <sup>c</sup>	PPV <sup>d</sup>	TP:FP	PPV	TP:FP	PPV	TP:FP	PPV
Trans_reg_C	0.12	7720	102:2282	0.04	1:30	0.03	0:0	–	0:0	–
CH	0.01	2960	167:4226	0.04	2:73	0.03	0:2	0.0	0:0	–
7tm_1	0.1	6302	358:28576	0.01	0:0	–	0:0	–	0:0	–
SH3_1	0.01	4160	74:674	0.10	7:60	0.10	0:5	0.0	0:0	–
Cadherin	0.06	7617	214:3333	0.06	1:46	0.02	0:7	0.0	0:0	–
Trypsin	0.1	6688	617:20312	0.03	0:0	–	0:0	–	0:0	–
Kunitz_BPTI	0.01	2130	86:799	0.10	11:48	0.19	0:2	0.0	0:0	–
KH_1	0.01	5114	78:1116	0.07	1:41	0.02	0:4	0.0	0:0	–
RRM_1	0.15	7684	119:1839	0.06	0:0	–	0:0	–	0:0	–
FKBP_C	0.01	5695	199:3445	0.05	0:10	0.0	0:1	0.0	0:0	–
Lectin_C	0.01	4479	234:4319	0.05	1:19	0.05	0:0	–	0:0	–
Thioredoxin	0.06	7483	188:4180	0.04	0:3	0.0	0:0	–	0:0	–
Response_reg	0.46	7613	202:5266	0.04	0:1	0.0	0:0	–	0:0	–
RNase_H	0.01	4782	271:7152	0.04	0:5	0.0	0:0	–	0:0	–
Ras	0.02	6390	329:11304	0.03	0:0	–	0:0	–	0:0	–
Pfam ID	#contacts /#sites <sup>c</sup>		$C_{ij}^s \geq r_t^b$		$r_t > C_{ij}^s > 0$		$0 > C_{ij}^s > -r_t$		$-r_t \geq C_{ij}^s$	
			TP:FP <sup>c</sup>	PPV <sup>d</sup>	TP:FP	PPV	TP:FP	PPV	TP:FP	PPV
Trans_reg_C	103/75	1.4	32:57	0.36	59:1584	0.04	12:669	0.02	0:2	0.0
CH	169/100	1.7	16:17	0.48	125:2454	0.05	28:1828	0.02	0:2	0.0
7tm_1	366/247	1.5	36:84	0.30	263:15695	0.02	59:12787	0.005	0:10	0.0
SH3_1	81/46	1.8	24:17	0.59	46:516	0.08	11:206	0.05	0:0	–
Cadherin	215/90	2.4	40:8	0.83	132:1519	0.08	42:1857	0.02	1:2	0.33
Trypsin	617/210	2.9	115:75	0.61	383:11331	0.03	119:8899	0.01	0:7	0.0
Kunitz_BPTI	105/51	2.1	16:12	0.57	55:575	0.09	26:262	0.09	0:0	–
KH_1	79/55	1.4	19:15	0.56	50:707	0.07	10:438	0.02	0:1	0.0
RRM_1	119/68	1.8	45:36	0.56	63:1257	0.05	11:546	0.02	0:0	–
FKBP_C	199/91	2.2	66:51	0.56	103:2114	0.05	30:1288	0.02	0:3	0.0
Lectin_C	243/102	2.4	36:13	0.73	160:2401	0.06	39:1923	0.02	0:1	0.0
Thioredoxin	188/99	1.9	53:61	0.46	109:2677	0.04	26:1442	0.02	0:3	0.0
Response_reg	202/110	1.8	72:87	0.45	101:3182	0.03	28:1988	0.01	1:10	0.09
RNase_H	271/127	2.1	37:56	0.40	161:3700	0.04	72:3387	0.02	1:14	0.07
Ras	329/158	2.1	81:55	0.60	203:6472	0.03	44:4768	0.01	1:9	0.10

<sup>a</sup> OTUs connected to their parent nodes with branches shorter than the threshold value  $T_{bt}$  are removed from each Pfam full alignment, and the number of remaining OTUs is listed.

<sup>b</sup> The  $r_t$  is a threshold for a correlation coefficient corresponding to the E-value  $E_t = 0.001$  (the P-value  $P_t = E_t/n_{\text{pairs}}$ ) in the Student's t-distribution of the degree of freedom,  $df = (2n_{\text{otu}} - 3) - 2$ , where  $n_{\text{pairs}}$  is the number of site pairs, and  $n_{\text{otu}}$  is the number of OTUs.

<sup>c</sup> TP and FP are the numbers of true and false positives, which are the number of contact site pairs and the number of non-contact site pairs in each category. Protein structures used to calculate contact residue pairs are listed in Table 1. Neighboring residue pairs within 5 residues ( $|i - j| \leq 5$ ) along a peptide chain are excluded in the evaluation of prediction accuracy. Also both terminal sites are excluded from counting in this table.

<sup>d</sup> PPV stands for a positive predictive value; i.e.,  $PPV = TP/(TP + FP)$ .

**Table 3.** Co-evolution score ( $\rho_{ij}^x$ ) based on each characteristic variable.

Characteristic variable	$\rho_{ij}^x \geq \rho_{ij}^s \geq r_t^a$			$\rho_{ij}^x \leq -\rho_{ij}^s \leq -r_t^a$		
	TP <sup>b</sup>	FP <sup>b</sup>	PPV <sup>c</sup>	TP	FP	PPV
	over all protein families					
Substitution	687	642	0.52			
Volume	18	20	0.47	73	10	<b>0.88<sup>d</sup></b>
Charge	6	8	0.43	134	54	<b>0.71<sup>d</sup></b>
Hydrogen bond	4	11	0.27	125	51	<b>0.71<sup>d</sup></b>
Hydrophobicity	23	13	<b>0.64<sup>d</sup></b>	23	16	<b>0.59<sup>d</sup></b>
$\alpha$ propensity	14	20	0.41	9	10	0.47
$\beta$ propensity	24	17	<b>0.59<sup>d</sup></b>	30	14	<b>0.68<sup>d</sup></b>
Turn propensity	21	18	<b>0.54<sup>d</sup></b>	17	15	<b>0.53<sup>d</sup></b>
Aromatic interaction	30	10	<b>0.75<sup>d</sup></b>	16	14	<b>0.53<sup>d</sup></b>
Branched side-chain	26	16	<b>0.62<sup>d</sup></b>	20	8	<b>0.71<sup>d</sup></b>
Cross link	23	12	<b>0.66<sup>d</sup></b>	5	9	0.36
Ionic side-chain	27	15	<b>0.64<sup>d</sup></b>	14	18	0.44

<sup>a</sup> See Eqs. 1 and 2 for the definition of  $\rho_{ij}^x$ . The  $r_t$  is a threshold for a correlation coefficient corresponding to the E-value  $E_t = 0.001$  (the P-value  $P_t = E_t/n_{\text{pairs}}$ ), in the Student's t-distribution of the degree of freedom,  $\text{df} = (2n_{\text{otu}} - 3) - 2$ , where  $n_{\text{pairs}}$  is the number of site pairs, and  $n_{\text{otu}}$  is the number of OTUs.

<sup>b</sup> TP and FP are the numbers of true and false contact residue pairs; protein structures used to calculate contact residue pairs are listed in Table 1. Neighboring residue pairs within 5 residues ( $|i - j| \leq 5$ ) along a peptide chain are excluded in the evaluation of prediction accuracy. Also both terminal sites are excluded from counting in this table.

<sup>c</sup> PPV stands for a positive predictive value; i.e.,  $\text{PPV} = \text{TP}/(\text{TP} + \text{FP})$ .

<sup>d</sup> These PPVs are larger than the PPV for concurrent substitutions, i.e., 0.52 for  $\rho^s$ .

Table 4. Accuracy of contact prediction based on the overall co-evolution score ( $\rho_{ij}$ ).

Pfam ID	#contacts /#sites <sup>a</sup>	TP + FP <sup>b</sup>	PPV <sup>c</sup>		MDPNT <sup>d</sup>		MDTNP <sup>e</sup>	
			DI <sup>f</sup>	$\rho_{ij}$	DI <sup>f</sup>	$\rho_{ij}$	DI <sup>f</sup>	$\rho_{ij}$
Trans_reg_C	111/76	27	0.556	<b>0.667</b>	1.30	<b>0.94</b>	4.20	<b>3.28</b>
	1.5	37	0.432	<b>0.622</b>	1.72	<b>1.16</b>	3.64	<b>2.82</b>
CH	172/101	43	<b>0.488</b>	0.465	<b>2.23</b>	2.55	4.59	<b>4.37</b>
	1.7	57	0.439	<b>0.491</b>	<b>2.12</b>	2.44	3.70	<b>3.30</b>
7tm_1	372/248	93	0.194	<b>0.344</b>	7.43	<b>5.31</b>	12.68	<b>7.71</b>
	1.5	124	0.169	<b>0.306</b>	7.30	<b>5.33</b>	12.18	<b>6.40</b>
SH3_1	89/48	22	0.636	<b>0.682</b>	0.83	<b>0.51</b>	<b>1.69</b>	2.34
	1.9	29	0.552	<b>0.655</b>	1.15	<b>0.62</b>	1.56	<b>1.51</b>
Cadherin	220/91	55	0.818	<b>0.836</b>	0.59	<b>0.25</b>	1.98	1.98
	2.4	73	0.753	<b>0.767</b>	0.64	<b>0.45</b>	1.60	1.60
Trypsin	636/212	159	0.591	<b>0.673</b>	1.75	<b>1.20</b>	3.26	<b>3.10</b>
	3.0	212	0.533	<b>0.613</b>	2.26	<b>1.65</b>	2.83	<b>1.94</b>
Kunitz_BPTI	111/53	27	0.444	<b>0.593</b>	1.40	<b>1.18</b>	2.31	<b>2.08</b>
	2.1	37	<b>0.541</b>	0.486	<b>1.13</b>	1.46	<b>1.86</b>	1.94
KH_1	90/57	22	0.500	<b>0.773</b>	0.99	<b>0.51</b>	<b>2.41</b>	3.29
	1.6	30	0.533	<b>0.700</b>	1.07	<b>0.56</b>	<b>2.16</b>	3.05
RRM_1	133/70	33	0.758	<b>0.818</b>	<b>0.52</b>	0.55	2.86	<b>2.36</b>
	1.9	44	0.705	<b>0.795</b>	0.83	<b>0.49</b>	2.49	<b>1.84</b>
FKBP_C	200/92	50	0.760	<b>0.840</b>	<b>0.53</b>	0.69	1.97	<b>1.85</b>
	2.2	66	0.697	<b>0.727</b>	0.94	<b>0.85</b>	1.66	<b>1.51</b>
Lectin_C	246/103	61	<b>0.770</b>	0.705	<b>0.80</b>	0.94	2.93	<b>2.67</b>
	2.4	82	<b>0.671</b>	0.646	1.19	<b>1.17</b>	2.54	<b>2.32</b>
Thioredoxin	188/99	47	0.532	<b>0.638</b>	0.98	<b>0.85</b>	3.43	<b>2.33</b>
	1.9	62	0.565	<b>0.645</b>	0.94	<b>0.91</b>	3.16	<b>1.86</b>
Response_reg	202/110	50	0.660	<b>0.680</b>	<b>0.86</b>	0.88	3.39	<b>3.06</b>
	1.8	67	0.642	<b>0.687</b>	1.01	<b>0.92</b>	2.54	<b>2.29</b>
RNase_H	273/128	68	<b>0.559</b>	0.471	<b>1.51</b>	1.53	<b>3.61</b>	5.44
	2.1	91	<b>0.549</b>	0.407	<b>1.55</b>	2.19	3.27	<b>3.07</b>
Ras	335/159	83	0.699	0.699	<b>0.94</b>	1.05	<b>2.98</b>	3.68
	2.1	111	0.631	<b>0.685</b>	<b>1.12</b>	1.45	<b>2.40</b>	2.51

<sup>a</sup> Protein structures used to calculate contact residue pairs are listed in Table 1. Neighboring residue pairs within 5 residues ( $|i - j| \leq 5$ ) along a peptide chain are not counted as contacts in the evaluation of prediction accuracy.

<sup>b</sup> TP and FP are the numbers of true and false positives; only predictions for TP + FP = #contacts/4 and #contacts/3 are listed.

<sup>c</sup> PPV stands for a positive predictive value; i.e.,  $PPV = TP / (TP + FP)$ . Better values are typed in a bold font.

<sup>d</sup> MDPNT stands for the mean Euclidean distance from predicted site pairs to the nearest true contact in the 2-dimensional sequence-position space [26]. Better values are typed in a bold font.

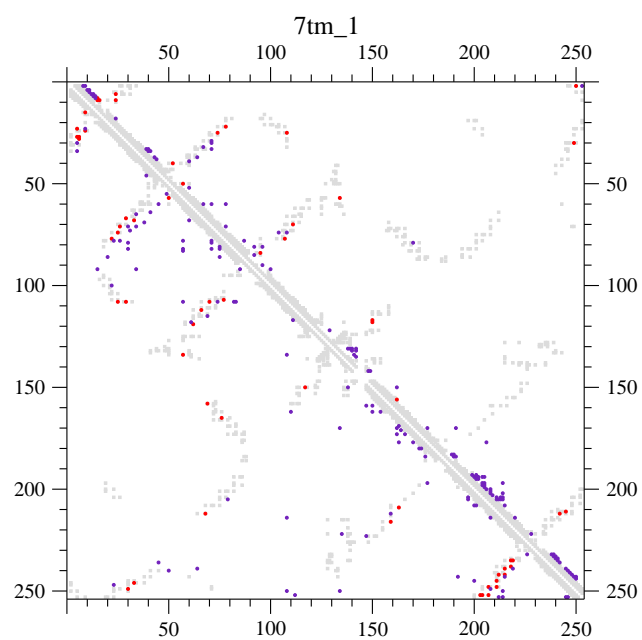
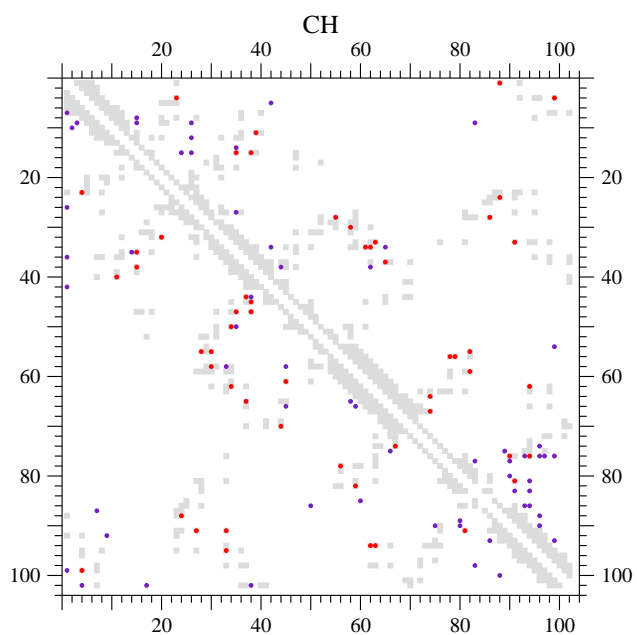
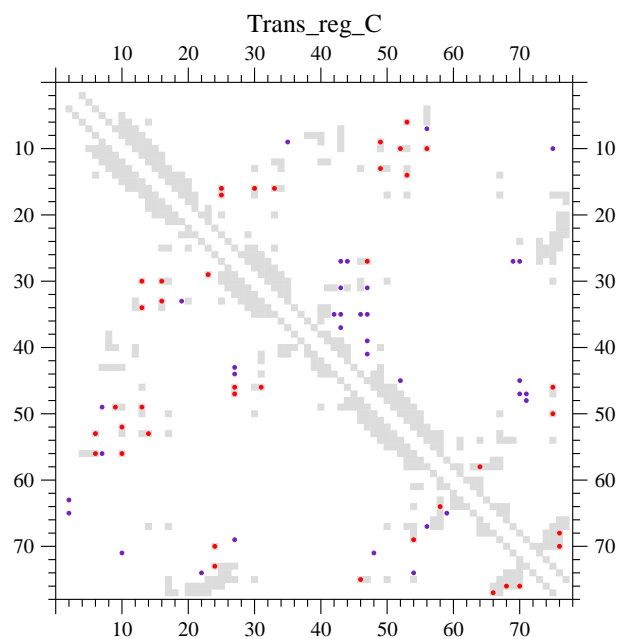
<sup>e</sup> MDTNP stands for the mean Euclidean distance from every true contact to the nearest predicted site pair in the 2-dimensional sequence-position space [26]. Better values are typed in a bold font.

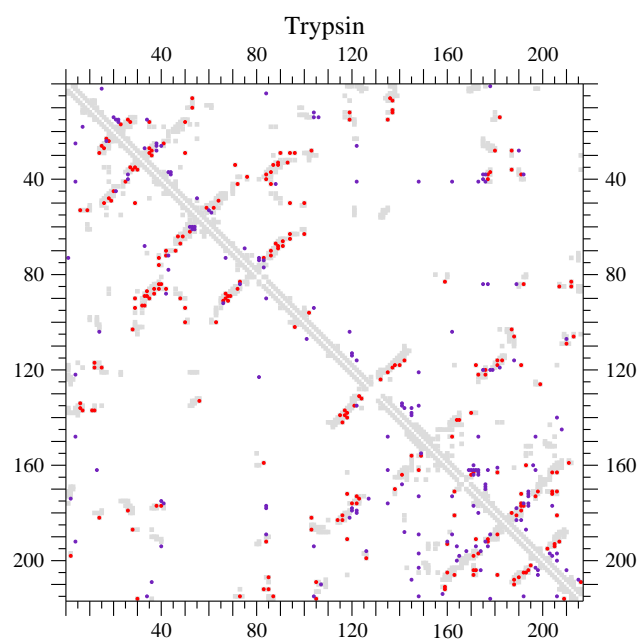
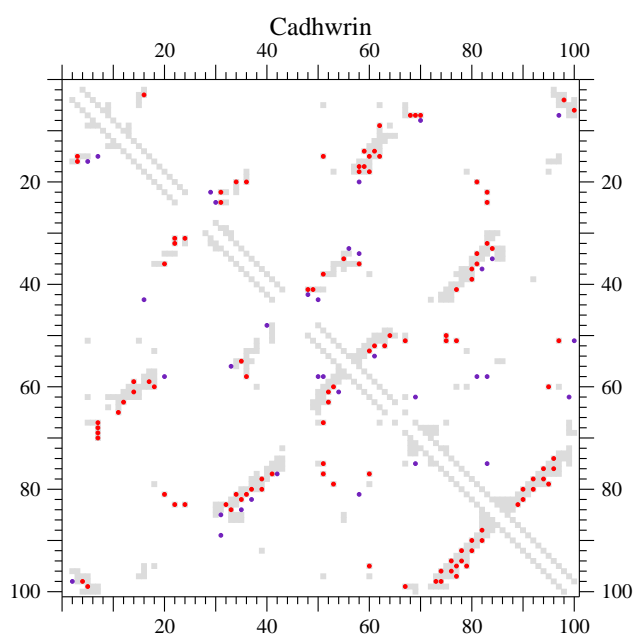
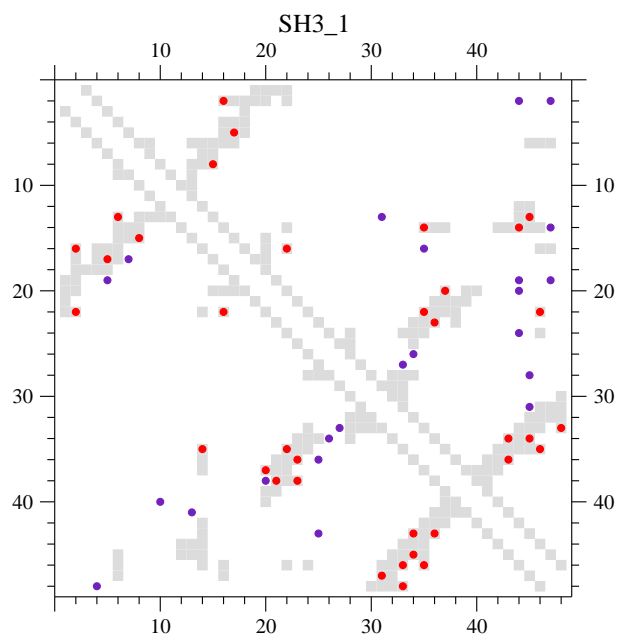
<sup>f</sup> DI means the prediction based on the direct information (DI) score published in [26]; a filtering based on a secondary structure prediction is not applied but only a conservation filter [26] is.

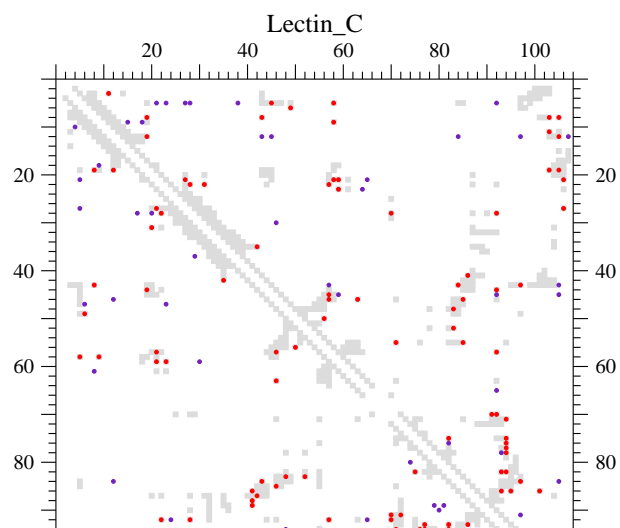
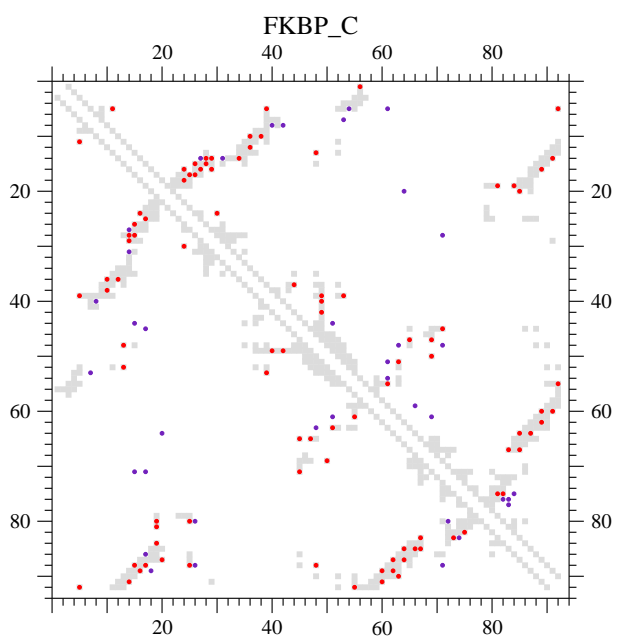
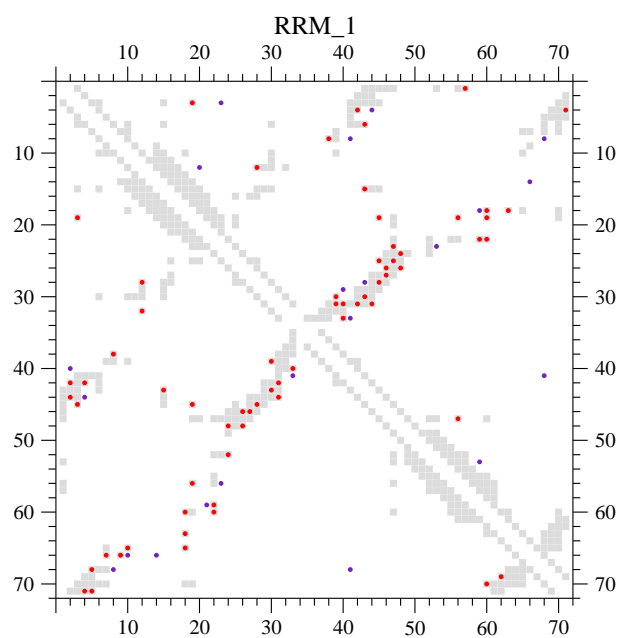
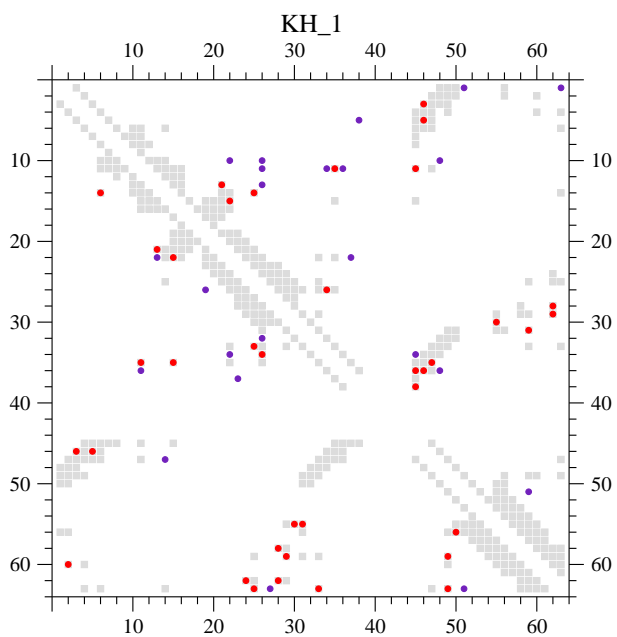
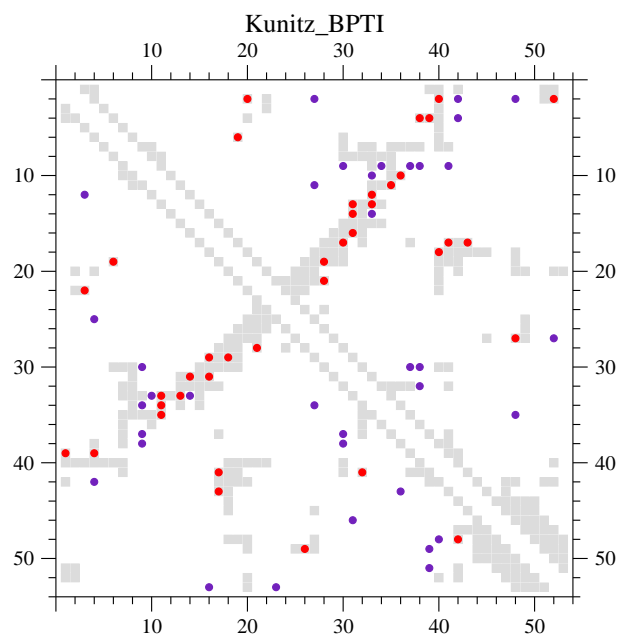
## Supporting Information

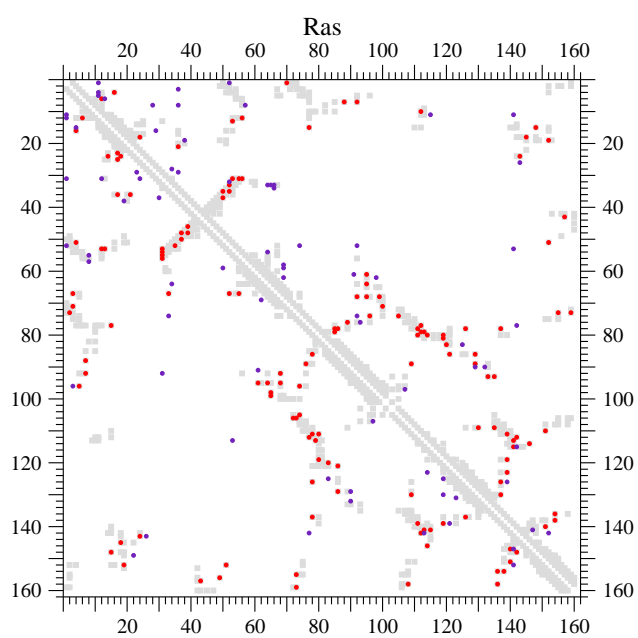
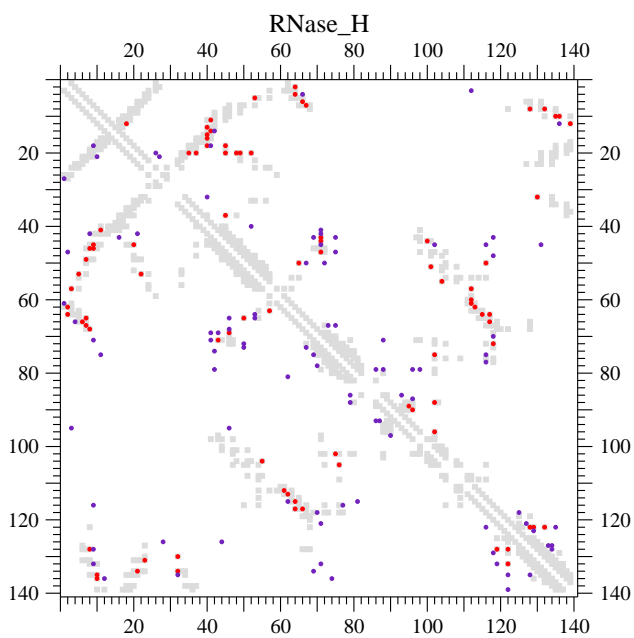
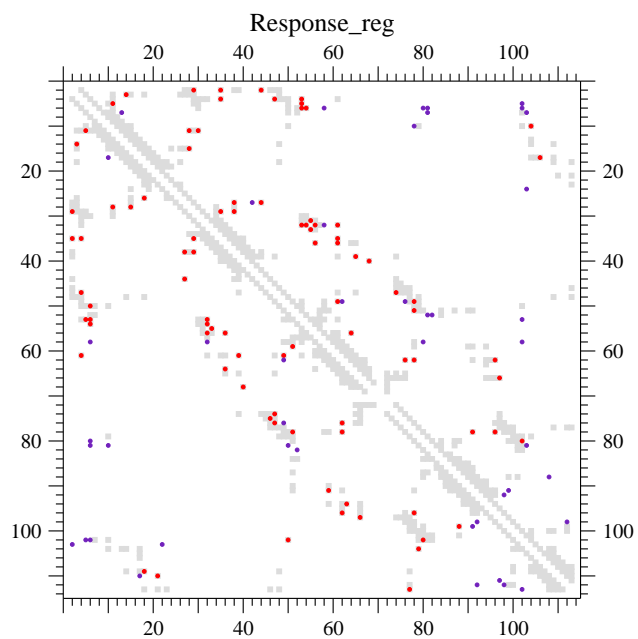
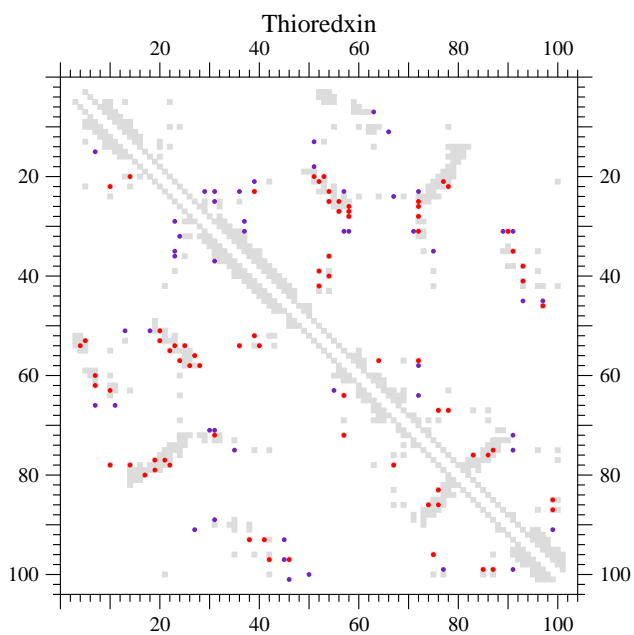
**Figure S1. Co-evolving site pairs versus DI residue pairs.** Residue pairs whose minimum atomic distances are shorter than 5 Å in a protein structure and co-evolving site pairs predicted are shown by gray filled-squares and by red or indigo filled-circles in the lower-left half of each figure, respectively. For comparison, such residue-residue proximities and predicted contact residue pairs with high DI scores in [26] are shown by gray filled-squares and by red or indigo filled-circles in the upper-right half of each figure, respectively; only the conservation filter is applied but the filters based on a secondary structure prediction and for cysteine pairs are not applied to the DI scores. Red and indigo filled-circles correspond to true and false contact residue pairs, respectively. Residue pairs separated by five or fewer positions in a sequence may be shown with the gray filled-squares but are excluded in both the predictions. The total numbers of co-evolving site pairs and DI residue pairs plotted for each protein are both equal to one third of true contacts ( $TP + FP = \#contacts/3$ ). The PPVs of both the methods for each protein are listed in Table 4.











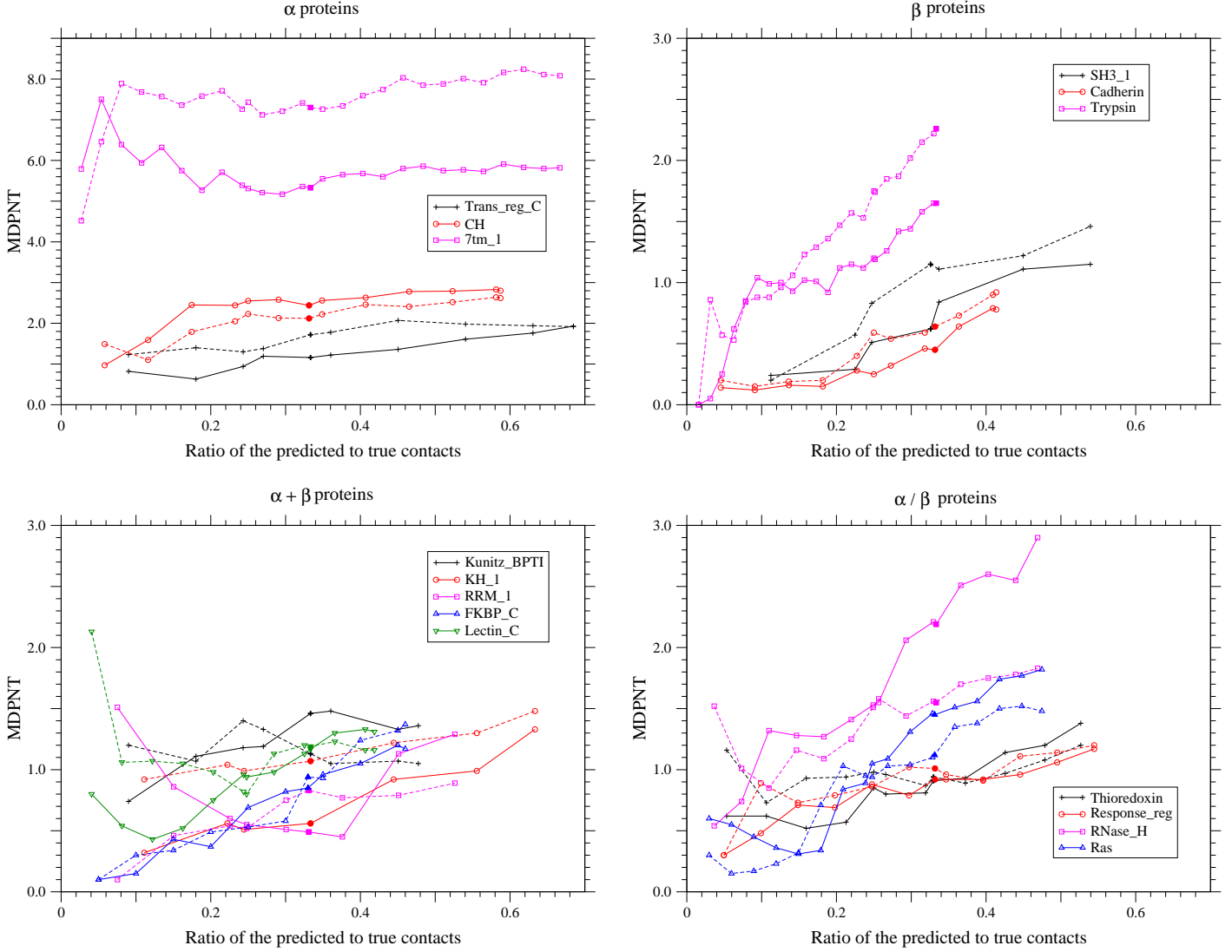


**Figure S2. Dependence of MDPNT on the number of predicted contacts.** The dependences of the mean Euclidean distance from predicted site pairs to the nearest true contact in the 2-dimensional sequence-position space on the total number of predicted contacts are shown for each protein fold of  $\alpha$ ,  $\beta$ ,  $\alpha + \beta$ , and  $\alpha / \beta$ . The solid and dotted lines show the MDPNTs of the present method and the method based on the DI score [26], respectively. The total number of predicted contacts is shown in the scale of the ratio of the number of predicted contacts to the number of true contacts. The total number of predicted site pairs takes every 10 from 10 to a sequence length; also MDPNTs for the numbers of predicted contacts equal to one fourth or one third of true contacts are plotted. The filled marks indicate the points corresponding to the number of predicted site pairs equal to one third of the number of true contacts. The number of sequences used here for each protein family is one listed in Table 1.

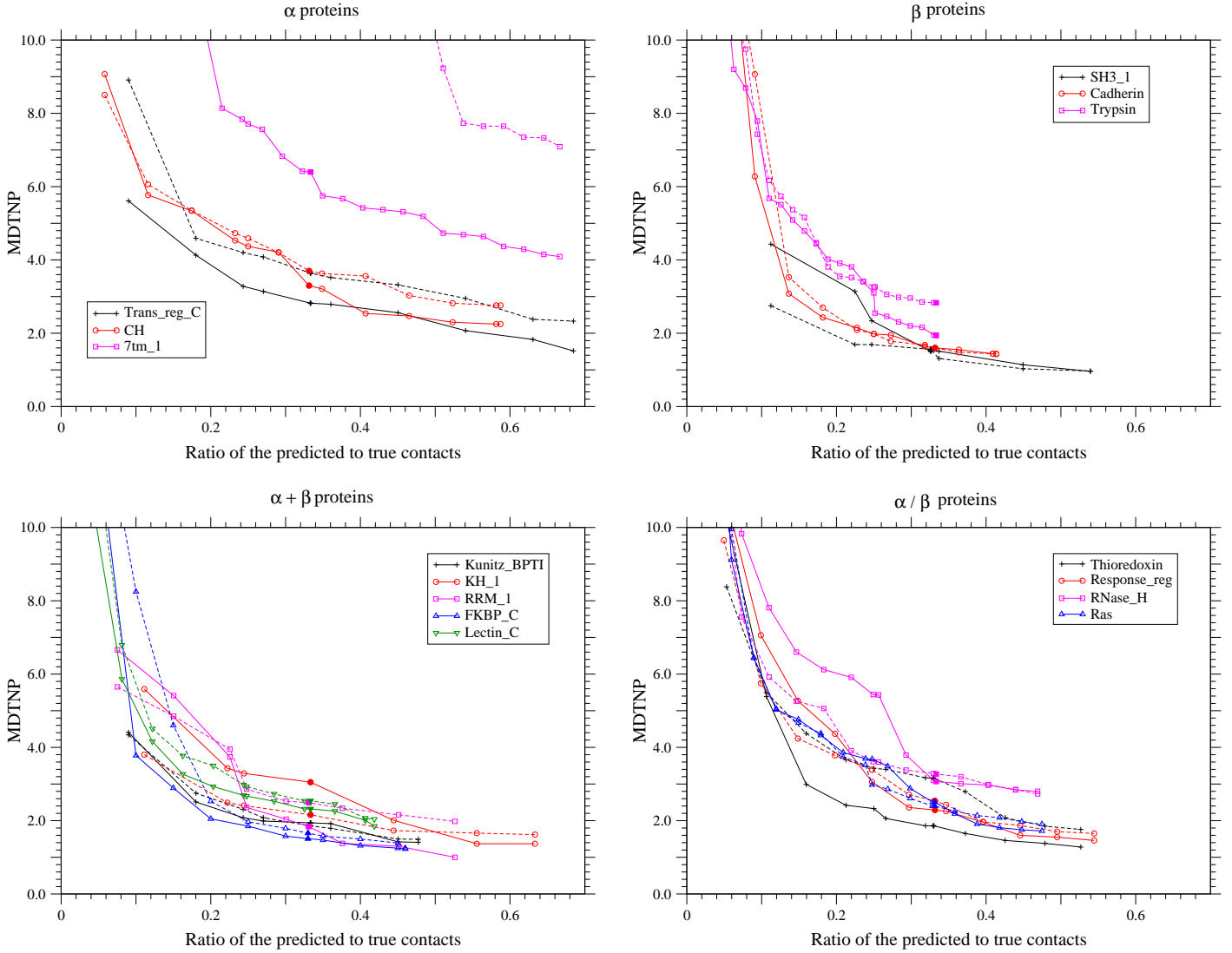


**Figure S3. Dependence of MDTNP on the number of predicted contacts.** The dependences of the mean Euclidean distance from every true contact to the nearest predicted site pair in the 2-dimensional sequence-position space on the total number of predicted contacts are shown for each protein fold of  $\alpha$ ,  $\beta$ ,  $\alpha + \beta$ , and  $\alpha / \beta$ . The solid and dotted lines show the MDTNPs of the present method and the method based on the DI score [26], respectively. The total number of predicted site pairs is shown in the scale of the ratio of the number of predicted site pairs to the number of true contacts. The total number of predicted site pairs takes every 10 from 10 to a sequence length; also MDTNPs for the numbers of predicted site pairs equal to one fourth or one third of true contacts are plotted. The filled marks indicate the points corresponding to the number of predicted contacts equal to one third of the number of true contacts. The number of sequences used here for each protein family is one listed in Table 1.



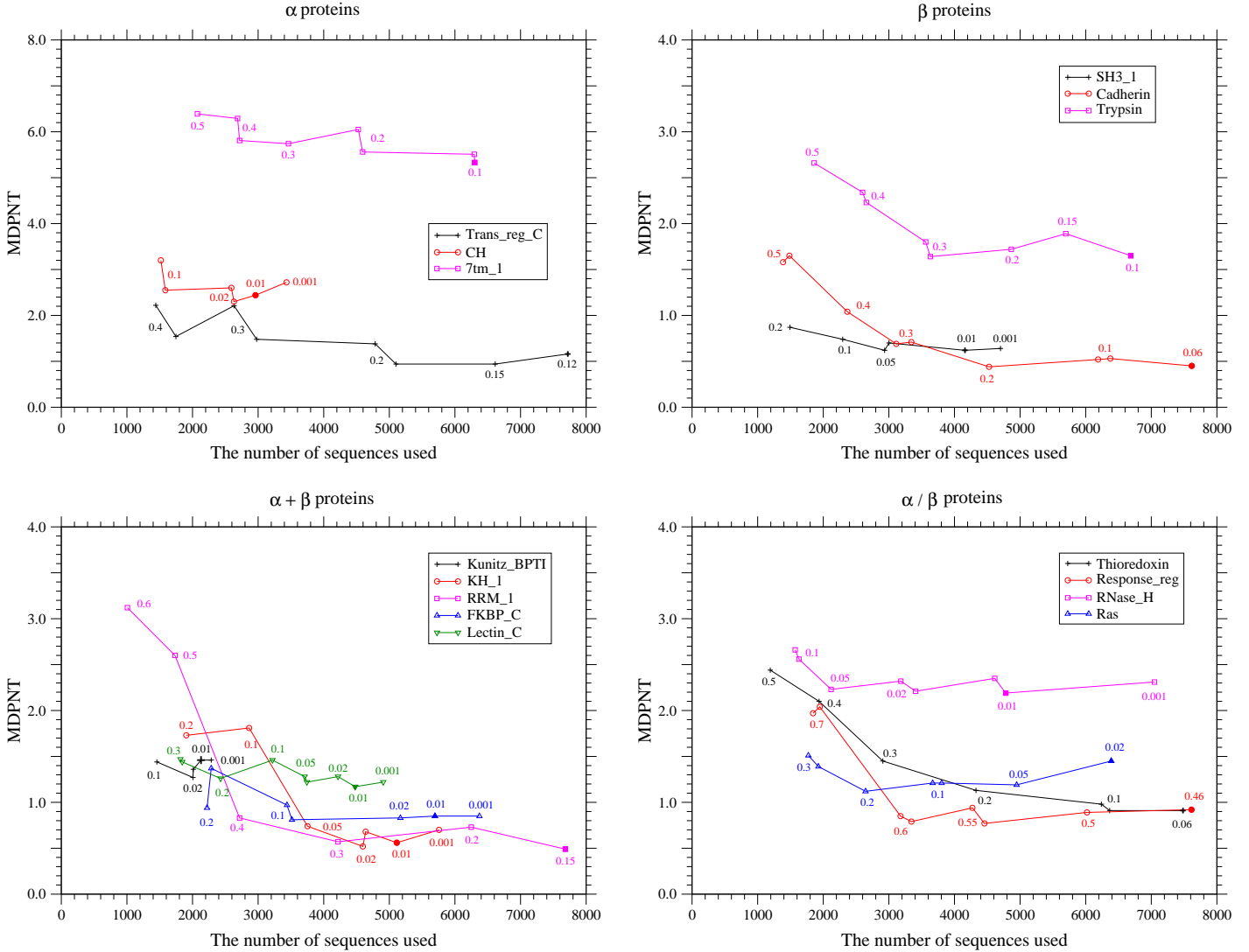


**Figure S4. Dependence of MDPNT on the number of sequences used.** The mean Euclidean distance from every predicted site pair to the nearest true contact in the 2-dimensional sequence-position space is plotted against the total number of homologous sequences used for each prediction. The filled marks indicate the points corresponding to the number of used sequences listed for each protein family in Table 1. The values written near each data point indicate the threshold value  $T_{bt}$ ; OTUs connected to their parent nodes with branches shorter than this threshold value are removed in the NJ tree of the Pfam full sequences used for each prediction. Some data points correspond to datasets generated by using the same value of the threshold but by removing different OTUs.

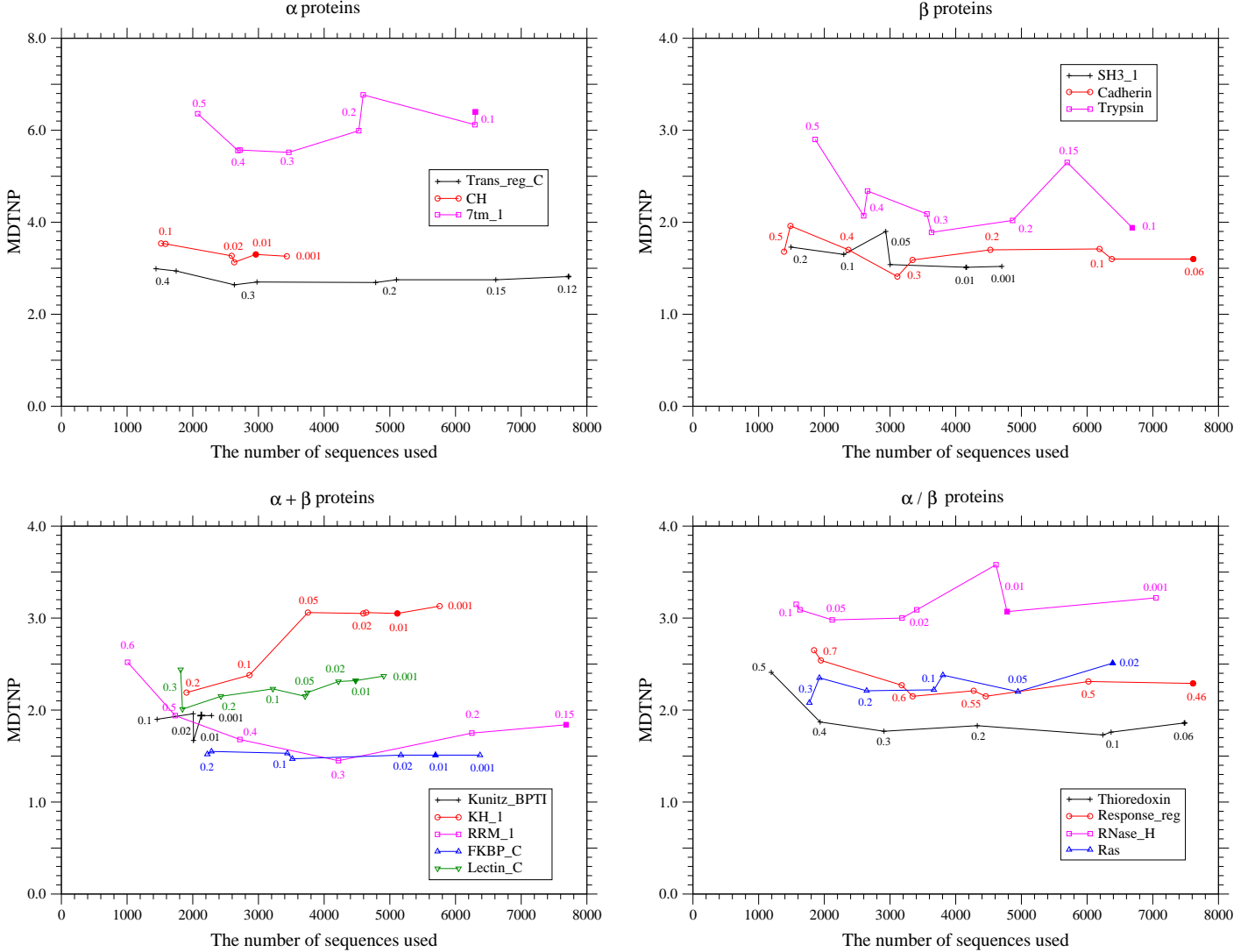


**Figure S5. Dependence of MDTNP on the number of sequences used.** The mean Euclidean distance from every true contact to the nearest predicted site pair in the 2-dimensional sequence-position space is plotted against the total number of homologous sequences used for each prediction. The filled marks indicate the points corresponding to the number of used sequences listed for each protein family in Table 1. The values written near each data point indicate the threshold value  $T_{bt}$ ; OTUs connected to their parent nodes with branches shorter than this threshold value are removed in the NJ tree of the Pfam full sequences used for each prediction. Some data points correspond to datasets generated by using the same value of the threshold but by removing different OTUs.